1966

A case study of data processing and wind parameters in relation to the U.s. Navy's numerical frontal analysis scheme.

Schardt, Delvin Leroy.

Monterey, California. U.S. Naval Postgraduate School

A CASE STUDY OF DATA PROCESSING AND WIND PARAMETERS IN RELATION TO THE U. S. NAVY'S NUMERICAL FRONTAL ANALYSIS SCHEME

DELVIN L. SCHARDT

A CASE STUDY OF DATA PROCESSING AND WIND PARAMETERS IN RELATION TO THE U. S. NAVY'S NUMERICAL FRONTAL ANALYSIS SCHEME

by

Delvin Leroy Schardt
Lieutenant, United States Navy
B. A., Doane College, 1961

Submitted in partial fulfillment

for the degree of

MASTER OF SCIENCE IN METEOROLOGY

from the

UNITED STATES NAVAL POSTGRADUATE SCHOOL

May 1966

ABSTRACT

The United States Navy's (USN) numerical front-location parameter, related to relative maxima in thermal-wind shear, as developed by Renard and Clarke, is investigated in its relation to the data-processing system used at the USN Fleet Numerical Weather Facility (FNWF), Monterey, California and to three front-associated wind parameters: a) geostrophic wind component normal to isentropes, b) shear of geostrophic wind component tangent to isentropes, and c) advective frontogenetical parameters. The study, which generalizes results to hyperbaroclinic zones and their boundaries, is carried out for the Northern Hemisphere at 1000, 850, 700, 500, and 300 mb for 00Z and 12Z, 20 August 1965, in the framework of FNWF's numerical analysis system.

Results indicate some major differences between the synoptic-scale baroclinic zones analyzed from radiosonde-observed temperatures, and FNWF's numerically processed mandatory-level virtual temperature data, at 1000 mb, over ocean areas, and at latitudes north of 55 degrees latitude. The normal geostrophic wind component was found to be useful in designating the type of front (cold, warm, stationary). Frontal shear proved to be mostly cyclonic at low levels (1000, 850 mb) becoming increasingly anticyclonic at higher levels (700, 500, 300 mb). The advective frontogenesis parameter appeared to be of limited value only. Where appropriate the numerical products are compared to the National Meteorological Center's frontal analyses.

TABLE OF CONTENTS

LIST OF TABLES AND FIGURES

LIST OF SYMBOLS AND ABBREVIATIONS

d	mesh length
i	central grid point to which $\Delta_{x,y}(\ )$ is applied
$i \pm 1, 2$	grid points 1 or 2 mesh lengths removed from central point
$\hat{k}$	unit vector along the local vertical
$\hat{\eta}_\theta$	unit vector in the direction of $\nabla\theta$
p	pressure
FG	frontogenesis = $-\nabla \mathrm{VNF} \cdot \nabla\theta$
FNWF	United States Navy Fleet Numerical Weather Facility, Monterey, California
GGθ	frontal parameter = $-\nabla\lvert\nabla\theta\rvert \cdot \hat{\eta}_\theta$
GGθo (GGθp)	= GGθ derived from observed (FNWF processed) temperatures
NPGS	United States Naval Postgraduate School, Monterey, California
SHVF	shear of the geostrophic wind component parallel to isentropes = $\nabla(\vec{V}_g \cdot \hat{k} \times \hat{\eta}_\theta) \cdot \hat{\eta}_\theta$
SS	static stability
T	temperature
USWB	United States Weather Bureau
VF	component of geostrophic wind parallel to isentropes
Vg	geostrophic wind
VNF	component of geostrophic wind normal to isentropes = $\vec{V}g \cdot \hat{\eta}_\theta$
VNFo (VNFp)	= VNF in relation to observed (FNWF processed) temperatures

Z_p	height of pressure level p
θ	potential temperature
$\nabla\theta$	horizontal gradient of potential temperature
$\nabla\theta_o(\nabla\theta_p)$	gradient of potential temperature using observed (FNWF processed) temperature
$\Delta_{x,y}(\ )$	finite difference of a parameter ( ) in x, y directions

1. Introduction

The need for an objectively specified front locator has prompted interested individuals at the United States Navy Fleet Numerical Weather Facility (FNWF) and United States Naval Postgraduate School (NPGS) to attempt a solution by numerical methods. [8] In their search for such a parameter Renard and Clarke tried various schemes. The one giving best results involves the second derivative of potential temperature. GGθ, the name given to the frontal parameter, is related to the shear vorticity of the thermal wind and may be symbolized as [1]

$$\frac{-\nabla|\nabla\theta|\cdot\nabla\theta}{|\nabla\theta|} = -\nabla|\nabla\theta|\cdot\hat{n}_\theta = -\partial^2\theta/\partial^2 n_\theta \qquad (1)$$

GGθ, as computed at FNWF, is based upon potential temperature (θ) determined from a unique radiosonde-data processing system which employs heights of seven mandatory pressure levels (Zp), and sea-level pressure. [5] A static stability parameter (SS), expressed as a function of Zp, is then derived for five layers (1000-775 mb; 775-600 mb; 600-450 mb; 450-300 mb; 300-200 mb). The SS is assumed constant in each layer, but is allowed to vary along a constant-pressure surface. Finally, virtual temperatures are computed at 3969 Northern Hemisphere grid points using the 1000-mb height, 1000/500 mb thickness and SS. Thus, the derived θ is a virtual potential temperature with the resulting fields hydrostatically consistent, statically

stable, and horizontally compatible. This particular θ (or T) is hereafter referred to as a processed θ (or T).

It is to be noted that although GGθ is used operationally to locate fronts numerically, the parameter is, in reality, a generalized baroclinic-zone locator. Figure 4 shows a typical FNWF analysis of GGθ, in this case the 850-mb level. Ridges and troughs in the GGθ field represent warm and cold boundaries of hyperbaroclinic zones, respectively, and as such are axes of maximum shear in the thermal wind. Since GGθ has been observed to have a direct relation to $\nabla\theta$, the intensity of GGθ at the baroclinic-zone boundaries gives an indication of the maximum strength of the baroclinic zone.

The warm-air boundaries of the hyperbaroclinic zones represent the numerical counterparts of conventional fronts. Figure 14 shows a typical relation between FNWF's numerically determined fronts (xxxx) and the USWB's hand-analyzed fronts (- - -). As may be noted, there is often a close comparison, especially in dense data areas. In other areas the two fronts are quite incompatible in orientation and/or location. Recent studies by Clarke and Renard and Hamrick have shown a need for improvement of the numerical front so as to be more in tune with hand-analyzed fronts. [1, 4]

2. Objectives and Outline of Study

This thesis study concentrated on two as yet unexplored areas of numerical-front analysis; 1) the effect of numerical processing on location and intensity of numerical fronts; and 2) the relation of pertinent wind parameters to the frontal analysis.

A comparison of the processed virtual temperature with reported radiosonde temperature was conducted by the author for the Northern Hemisphere at five levels: 1000 mb, 850 mb, 700 mb, 500 mb, and 300 mb. A similar comparison was also made for the GGθ fields derived from the two temperature fields.

Fronts as used operationally by synoptic meteorologists are associated with unique wind phenomena. Presently, FNWF's numerical-front model does not incorporate any wind parameters. In this paper three such wind parameters, as determined numerically, are investigated in association with both the computerized and manually-analyzed fronts and baroclinic zones.

The first of these wind parameters considered was the component of the geostrophic wind normal to the isentropes (VNF) on an isobaric surface, where the isentropes, of necessity, are regarded as a best approximation to the orientation of the fronts. This is expressed as:

$$VNF = \vec{V}_g \cdot \frac{\nabla\theta}{|\nabla\theta|} = \vec{V}_g \cdot \hat{n}_\theta \qquad (2)$$

Since the motion of a front is generally taken as the component of wind normal to it, the movement of numerical fronts should be statistically related to VNF.

Second, the frontogenical properties of a numerically determined front may be indicated by: [6]

$$FG = -\nabla\left(\vec{V}_g \cdot \frac{\nabla\theta}{|\nabla\theta|}\right)\cdot\nabla\theta = -\nabla\left(\vec{V}_g\cdot\hat{\eta}_\theta\right)\cdot\nabla\theta \qquad (3)$$
$$= -\nabla(VNF)\cdot\nabla\theta$$

Since $GG\theta$ is well correlated with baroclinicity, time changes in the magnitude of $GG\theta$ may be used as a measure of frontogenesis in order to verify the applicability of equation (3).

The third wind parameter considered was shear of the geostrophic wind component parallel to the isentropes on an isobaric surface:

$$SHVF = \nabla\left(\vec{V}_g \cdot \hat{k} \times \frac{\nabla\theta}{|\nabla\theta|}\right)\cdot\frac{\nabla\theta}{|\nabla\theta|} \qquad (4)$$
$$\equiv \nabla\left(\vec{V}_g \cdot \hat{k} \times \hat{\eta}_\theta\right)\cdot\hat{\eta}_\theta$$

Horizontal wind shear is a parameter often used to locate conventional fronts, and so the relation of shear to both the baroclinic zone and its warm-air boundary is considered here.

The study of these various wind parameters was carried out for all five of the previously mentioned levels, for both the FNWF processed temperatures and the observed temperatures at two radiosonde reporting times.

3. Data and Charts

Data and chart material for the whole Northern Hemisphere, collected at 0000Z and 1200Z 20 August 1965, were utilized for this study. The selection of these times was purely arbitrary in that no unseasonable weather conditions influenced their choice. For certain portions of the study, only the dense-data areas of the North American Continent and North Atlantic Ocean were utilized. The basic chart used is the 1:30,000,000 polar stereographic Northern Hemisphere projection with data at 63 x 63 grid points, each 381km apart at 60 N.

The chart material consisted of θ, $\nabla\theta$, $GG\theta$, VNF, FG, and SHVF obtained from both the FNWF processed virtual temperature and observed temperature data. The latter were obtained from FNWF listings of mandatory-level temperature data. These observed temperatures were extracted from the data printouts, put on punch cards and numerically analyzed at FNWF, using the processed temperature fields as first guess.

Rather extensive procedures were adopted to uncover errors in transcribing data from listings and punch cards. The fields of analyzed temperatures and differences in processed and observed temperatures were carefully screened for indication of errors in the observed temperature fields.

Numerical differentiation of wind and temperature parameters was accomplished by a finite differencing technique employing the quartic interpolation polynomial in the form

$$\Delta_{x,y}(\ ) \text{ at } i=0$$
$$= \frac{1}{12d}\left\{(\ )_{i-2} + 8\left[(\ )_{i+1} - (\ )_{i-1}\right] - (\ )_{i+2}\right\} \qquad (5)$$

After the 12Z 20 August 1965 observed temperature charts had been analyzed for frontal phenomena, it was discovered that an improper guess field had been used. A reanalysis of these temperatures using a corrected guess field, showed insignificant changes from the initial temperatures for grid points north of 15 N, so the 12Z chart material as originally run, was accepted.

4. Temperature: FNWF Processed vs. Observed

To determine the difference between the FNWF processed (virtual) temperature and the observed temperature, the latter was subtracted from the former at each grid point. Since the FNWF temperatures are virtual, while the observed are not, differences of 0.0 C to +3.0 C are to be expected.

The resulting temperature differences were categorized by level, locale, and magnitude. The stratification by location involved a latitudinal grouping (South, 20 N - 35 N; Central, 35 N - 55 N; and North, 55 N - 90 N), and a longitudinal grouping (North America, 70 W - 130 W; Pacific, 130 W - 140 E; Asia, 140 E - 60 E; Europe, 60 E - 10 W; Atlantic, 10 W - 70 W). Figure 1 shows the limits of these various areas. The number of grid points within each area is given alongside the title of each area.

Temperature differences for 00Z 20 August 1965 are tabularized by per cent of grid points (see Table 1). It can be noted from the table that the South area has the greatest per cent of grid points in the 0.0 to +2.9 range and the least in the -0.9 to 0.0 column at all levels. Except for 500 mb, the reverse is true of the North area. These figures merely reflect the normal meridional gradient of moisture and give reason for the over-all larger $\nabla\theta$ and $GG\theta$ using the FNWF vice the observed temperatures. Differences $\geq +3.0$ C and < -0.9 C are not explainable in terms of moisture nor may they be regarded as negligible "noise" differences. Such cases amount to an average of 11, 12, and 20% in the South, Central, and North zones, respectively, for all levels except 1000 mb, while 1000 mb shows 37, 55, and 44% of cases in the three zones, respectively. 1000 mb, of course, is more often than not a fictitious atmospheric level and this may account for the discrepancies, while such things as mislocated data, transmission errors, processing errors, and so forth, account for the remainder.

When the longitudinal division of area is employed, the high moisture content of the air above water surfaces is evidenced by the higher percentages over the Pacific and Atlantic in the 0.0 to +2.9 range, especially at 850 and 1000 mb (Table 2). As already indicated above, 1000 mb shows the maximum differences, while the Asiatic area is noted to have the greatest percentage of large temperature differences at all levels.

Thus, collectively, the two tables suggest that GGθp and GGθo fields are most likely to differ at the 1000-mb level, at latitudes poleward of 55 N, and over the Asiatic area 60 E - 140 E.

Ferrentino, in a climatological study, made a similar comparison of temperature differences for the same observation time at the 200, 500, and 850-mb levels. [3] He initially converted the observed temperatures to virtual temperatures and calculated differences from the FNWF-processed temperatures at reporting stations only. His findings indicated that the 500-mb level was the best of the three levels tested, with 80 per cent of the stations having a difference within plus or minus 1.2 C. This result is in good agreement with Tables 1 and 2, which show the least percentage of unexplainable large temperature differences at 500 and 700 mb.

5. GGθ Analyses

Criteria Used in the Analysis of GGθ Isolines, Ridges, and Troughs

Values of GGθ were computed and printed out on the FNWF 63 x 63 square grid (as were all other parameters being considered) in units of $10^{-2}C/(100km)^2$. Both positive and negative GGθ areas are indicated (Fig. 2-11) by isolines drawn on Northern Hemisphere 1 : 30,000,000 polar stereographic projections at intervals of 10 units starting with the 5 line. GGθ values are generally less than 35 units. Closed contours were not drawn around <u>single</u> grid point values $\geq |5|$ units of GGθ.

The main requirement for the placement of fronts (i.e., GGθ ridges or warm-air boundaries of baroclinic zones) on the contoured GGθ fields was that the front be associated with a baroclinic zone that had a well defined rear (cold-air) boundary. Thus, in order for a ridge in the GGθ field to be indicated, it must have an associated trough, with both ridge and trough meeting certain necessary requirements, as follows. Ridges and troughs were only drawn within an area of GGθ where magnitudes exceeded five units. An exception to this rule occurred when two distinct ridge lines, aligned end to end, were separated by a small distances of less than two mesh lengths having values between zero and +5 units. This exception was not allowed if the trough line was also discontinuous in the same fashion. This rule was also made applicable to trough lines if they were separated by a similarly small distance of negative values. Areas of positive and negative GGθ that qualified, but were circular in shape, such that distinct ridges or troughs could not be discerned, were also not analyzed for these entities. No distance limitations between ridge and trough were used, but ridges and troughs were required to be approximately parallel.

The reason for the preceding limiting conditions was to specify an objective means of locating only the synoptic-scale fronts. It can also be seen that if all GGθ ridges, without further refinement, were classified as fronts, the number and

mileage of numerically-determined fronts would far exceed that for operationally produced hand-analyzed fronts, resulting in a situation not entirely desirable for this study.

Comparison of GGθp, GGθo, and USWB Fronts at 00Z 20 Aug 1965

A descriptive comparison of the two GGθ fields, derived from FNWF processed (GGθp) and observed (GGθo) temperatures, for 00Z at five mandatory levels, is given below.

(1) 1000 mb (Figs. 2, 3)

The fronts indicated by the two GGθ fields are basically in very poor agreement, a situation somewhat expected from the results shown in Tables 1 and 2. The GGθo fields show a very limited number of closed centers over ocean areas, while the GGθp field has centers over ocean areas, but decreased intensity compared to land areas. The fronts along the western part of North America, for which there is some correlation between the two charts, are probably a result of diurnal heating and the trade wind inversion, a phenomena peculiar to the West Coast, especially during summer.

(2) 850 mb (Figs. 4, 5)

The locations and intensities are in good agreement, especially over eastern United States. Relation of the two fields is particularly poor poleward of 55 N in the North American Arctic. Intensities of GGθo remains less than GGθp over oceans. Inversion and diurnal heating effects appear to continue domination of the North American west coast.

(3) 700 mb (Figs. 6, 7)

This level shows more frontal mileage than lower levels, mostly due to increases over ocean areas. Agreement of fronts has improved over 850 mb. The United States west coast baroclinic zone has changed orientation. 700 mb is normally above the trade wind inversion.

(4) 500 mb (Figs. 8, 9)

Overall intensity on both charts is large with $GG\theta p$ values greater than $GG\theta o$. Agreement of position and number of fronts is better than at lower levels. Whereas lower levels featured short-segmented fronts, there are now extensive frontal bands. Low latitude frontal bands are now quite evident.

(5) 300 mb (Figs. 10, 11)

A marked increase of intensity compared to lower levels is noted for each field; also fronts are more continuous. The greatest variation in front location from Figures 10 and 11 is shown over China. The low-latitude baroclinic zone system is well developed.

The position of the fronts at the five levels, for processed and observed temperatures, are given in Figures 12 and 13, respectively. For processed temperatures, the frontal contours that lie over the eastern United States, Canada, northern Atlantic, northwestern Europe, and central Asia are internally consistent. Slopes range from 50 : 1 in the cold front sector to 150 : 1 in the warm front sector. Such correspondence is not as evident in the observed

frontal contours. In areas other than those mentioned above, a display of vertically consistent slopes on both charts is not so evident. Numerous occasions of intersecting frontal contours and fronts sloping toward warm air with increasing height are noted. The two figures make obvious the poor fit of 1000-mb fronts with those at other levels.

When GGθo and GGθp fronts are compared with USWB fronts for 850 mb (Fig. 14), a closer comparison between GGθo and GGθp fronts exists than between USWB fronts and either of the GGθ fronts Incompatabilities occur for USWB occlusions and east ocean-area fronts, and GGθ fronts over western North America and Africa.

Comparison of Frontal Positions at 00Z and 12Z 20 Aug 1965

Figure 15 shows the position of GGθp fronts and USWB fronts for 00Z and 12Z. In areas where the two may be associated, such as eastern North America, western Europe, and the west Pacific similar 12-hour frontal movements are noted.

Summary

In summarizing the differences that occur between the two GGθ fields, the weak GGθo baroclinic zones over water for the lower levels were most obvious. The GGθp zones are relatively stronger due to processed temperatures being virtual temperatures. In effect, when crossing from the rear to the front of a transition zone, that is from cold dry air to warm moist air, the temperature range for observed temperatures is less than that for processed

temperatures. This reduction of temperature range directly decreases the intensity of $GG\theta o$. At upper levels, the air contains less moisture, and consequently this variation between $GG\theta o$ and $GG\theta p$ does not occur.

Fronts found at 700 mb and at higher levels were indicated by both $GG\theta$ fields. The existence of upper-level fronts has been explained as intrusions of stratospheric air into the troposphere through breaks in the tropopause. [7] These intrusions were observed in polar air. The upper-level $GG\theta$ fronts, which occur in tropical air, are possibly associated with the tropopause break surrounding the sub-tropical jet stream.

6. VNF Analyses

Introduction

In applying equation (2) it was assumed that isentropes are aligned with $GG\theta$ ridges. A check at all levels, for both processed and observed temperatures, showed this to be a very good approximation. With reference to Figure 16, showing a cold-front situation at 700 mb, the following explains schematically the positive and negative zones in the VNF field. Here, since the geostrophic component, VNF, is directed along $\hat{\eta}_\theta$, VNF is positive. For warm front case, VNF and $\hat{\eta}_\theta$ are oppositely directed and hence VNF is negative.

The relation of actual frontal movement to the component of geostrophic wind normal to isentropes, formed from both processed

temperatures (VNFp) and observed temperatures (VNFo), for the period 0000Z to 1200Z, was studied. Figure 17 shows a typical VNFp pattern over North America and the North Atlantic at 850 mb for 0000Z, with contours at 0, $\pm$2.5, $\pm$5.0, and $\pm$10.0 meters/sec. Warm and cold air boundaries of baroclinic zones are also indicated, so that their relation with the VNF field may be noted. Fronts of any significant length are seen to be crossing repeatedly through positive and negative areas of VNFp, which, in general, are cellular in shape.

Comparison of VNFp to GGθp Baroclinic Zones
at 00Z and 12Z 20 August 1965

The relation of VNFp to the processed-temperature GGθ fronts, at the five mandatory levels for the 12-hour period, will be discussed first. Since 850 mb offers a good description of the existing large-scale conditions near the surface, without undue modification resulting from surface influences, it will be discussed in greater detail. Variations from 850 mb phenomena will be emphasized in the discussion of the other levels.

(1) 850 mb (Figs. 17, 18, 19)

Figures 17 and 18 show the VNFp pattern and the fronts for times 00Z and 12Z, respectively. An alternation of positive and negative VNFp centers along the front occur at both times. As expected from the VNF pattern along the baroclinic zone, the amplitude of the frontal wave increases during the period (see Fig. 19).

A traveling frontal wave is indicated by the movement of negative and positive VNFp centers during the period. To wit, the positive area of VNFp, having its greatest intensity over James Bay in Canada at 00Z, moves south southeastward to within the baroclinic zone over northern New York state by 12Z; the negative center,just off Nova Scotia and Newfoundland at 00Z, moves northeastward to just east of Newfoundland by 12Z. This movement, which averaged close to 40 knots, and movement of other pertinent VNFp centers, is shown by history positions on the 12Z chart.

All VNFp positive and negative areas having at least one closed contour at 00Z were found to have counterparts at 12Z, except for two centers located in the extreme northeastern corner of the area, which most likely moved out of our area of study. New centers can sometimes be traced to previous centers that have split.

The relation of VNFp to frontal movement was checked by selecting points within the hyperbaroclinic zone and then calculating the average VNFp and actual movement experienced by these identifiable points during the 12-hour period. Of nine uniformly distributed points, eight moved in the direction indicated by the 12-hour average of VNFp. The magnitude of VNFp was also a good indicator of the amount of movement.

(2) 1000 mb (Figs. 20, 21)

The VNFp field for this level has the characteristic alternating VNFp centers along the front. The vertical consistency between 1000 mb and 850 mb is quite good at both 00Z and 12Z, except for a small area just off Nova Scotia. The intensity of the closed centers at 1000 mb is slightly below the intensity of the 850 mb centers. Time consistency at the former is less favorable than that of 850 mb. The relation of VNFp to movement of the baroclinic zone showed that of six baroclinic-zone points checked, only three showed direction of movement indicated by VNFp.

(3) 700 mb (no Figs. shown)

Counterparts of all major centers at 850 mb are observed at 700 mb, with little change in intensity or shape for both observation times. Time consistency for this level is good in spite of an increased amount of splitting and combining of centers during the 12-hour period. Negative centers tended to be more intense than positive centers. Seven out of ten points in the transition zone showed agreement of VNFp to baroclinic zone movement.

(4) 500 mb (Figs. 22, 23)

The time consistency for this level has deteriorated from that of lower levels. In conjunction, the degree of space continuity with lower levels has fallen off. The intensity values of centers has gone unchanged from 700 mb. VNFp was an indicator of direction of movement at only five of eight baroclinic-zone points investigated.

(5) 300 mb (no Figs. shown)

A marked increase of intensity of VNFp centers relative to lower levels is the result of a sharp increase in the Vg, and not a more normal alignment of Vg to to the isentropes. An increase of centers with decreased sizes was also noted. The tracing of VNFp centers from one observation time to the next is more difficult, and only partial space continuity exists. VNFp is not a good indicator of front movement due to probable non-linear fluctuations of VNFp within the observation period.

Comparison of VNFo to GGθo Baroclinic Zones
at 00Z and 12 Z 20 August 1966

The comparison of VNFo with the observed temperature GGθ front movement is presented for two levels only, 850 mb and 500 mb.

(1) 850 mb (Figs. 24, 25, 26, 27)

Figures 24 and 25 show the VNFo field in relation to the warm-air baroclinic-zone boundaries for the two observation times. The alternation of VNFo centers along the front is similar to that detected for the processed temperature charts (Figs. 17, 18, 19). Since the same Vg field is used for both VNFs (processed and observed) for a given time, differences between the two must result from differences in the two $\nabla\theta$ fields. Figure 26 shows a comparison of the two VNF fields for 00Z. The only major differences are those near Greenland and over the extreme northeast Atlantic.

As shown by Figure 27, there is an outstanding time consistency of VNFo centers for the time period. Positive centers generally

show a south and east movement, while negative centers show a north and east movement, similar to that observed for processed temperature VNF centers. However, the expected increase in amplitude of the 12Z fronts does not materialize, although most of the North American-North Atlantic frontal systems do move in accordance with the VNFo fields.

(2) 500 mb (no Figs. shown)

The time continuity of the VNFo centers has fallen off considerably when compared to the lower levels. Space continuity from the 850-mb level is quite limited. Only along small sections of the front can VNFo be considered an accurate indicator of front movement.

Comparison of VNF Fields with USWB Fronts

When VNF fields derived from processed and observed temperatures were compared with USWB fronts, only the 850-mb level was considered. This limitation was due to the fact that the USWB operationally produces only 850-mb and surface analyses of fronts.

The VNFp centers were excellent indicators of the instantaneous movement of USWB fronts for all portions except for the extension into Texas (Figs. 28, 29). The USWB front at 00Z has a wave structure which increased in amplitude; eastward progression of this wave was well indicated by the location and movement of the VNFp centers. This is shown in fine detail along the front in the North Atlantic.

When the VNFo field was compared to the USWB fronts for the 850-mb level, a high degree of relationship prevailed (Figs. 30, 31); however, it was not as profound as that obtained using the processed-temperature VNFs.

Summary

In summary, it was noted that when a front came under the influence of an alternating VNF field, the front tended to develop a progressive wave-like structure. This phenomena, which is known to exist in nature, was most evident at 850 mb, using processed temperature. The VNF fields for both processed and observed temperatures had time continuity at each level and space continuity between levels, except at 300 mb. This upper level also had comparatively smaller centers along with an increase in intensity. When the 850-mb VNF was applied to the USWB fronts for this level, a high degree of correlation with the front movement existed, especially when using processed temperatures.

7. FG Analyses

The expression used for frontogenesis (FG) here (equation 3) is an advective one, which in effect, assumes conservation of temperature by individual air particles. Values of FG were computed numerically at grid points and expressed in units of 0.781 x 10^{-6}C/(100km)/sec. Figure 32 shows the results obtained at 850 mb using processed temperatures. The larger values of FG are situated within the hyperbaroclinic zone, and rightly so, as FG is

proportional to $\nabla\theta$. Intense centers of FG, at all levels, showed good time continuity. This was true of space continuity also, which was best between 850 and 700 mb.

It is to be noted that the FG values are instantaneous quantities, however time-integrated values are of interest for comparison to changes in the GGθ field. In order to assess the relation of FG to changes in GGθ along the numerical front, it was assumed that if a grid point was experiencing positive FG at both the beginning and the end of a 12-hour period, it experienced positive FG throughout. The same is assumed of grid points having negative values (i.e., frontolysis). If a grid point experienced a negative (positive) value initially and a positive (negative) value at the end of the period, it was not considered in the evaluation. Figure 33 is a 1000-mb depiction of North American and North Atlantic areas having constant algebraic sign of FG during the 12-hour period, 00Z to 12Z 20 August 1965. It can be seen that about two thirds of the area showed no change in algebraic sign of FG. This percentage, to within 10 per cent, applies to all other levels, except 300 mb, which had a markedly decreased percentage.

The evaluation is summarized in Table 3, which shows the per cent of FNWF grid points at which time variations in $\nabla\theta$ agree and disagree with the FG calculations. Frontogenesis (frontolysis) occurs when $\nabla\theta$ increases (decreases) during the period. 300 mb

is not included due to the numerous points showing changes in sign of FG during the period, thereby giving few grid points for verification.

The results given in Table 3 imply that the computed positive FG is not a good indication of frontogenesis, although negative FG (i.e., frontolysis) is more promising, especially at the lower free-atmosphere levels of 850 and 700 mb. An explanation of this may be that a certain amount of frontogenesis is needed to maintain a mature baroclinic zone against such non-advective frontolytical processes as radiation, conduction, convection, and mixing, whereas frontolysis is associated with a definite decrease in the intensity of $\nabla\theta$ as the non-advective processes are frontolytical in character. With regard to FG indicating formation as well as intensification, the FG pattern at 500 mb for 00Z was indeed a good indicator of baroclinic-zone formation by 12Z in the North Atlantic. But in other areas the relation was not so good.

The better results at 850 and 700 mb give evidence that advective frontogenical processes are the prime factors at lower levels as noted by Sanders. [9] But then why doesn't 1000 mb have the best verification? This may result from the geostrophic wind being a poor representation of the surface wind, or from the 1000 mb surface being a fictitious atmospheric level in many cases. Another explanation is that non-conservative influences on the temperature, such as surface heating and turbulent mixing, are most intense below 850 mb. [2]

This particular evaluation method considered grid points in a fixed coordinate system, an Eularian approach. A Lagrangian approach ought to give better results. This was tested by selecting "identifiable points" midway between the baroclinic-zone boundaries and checking the time variations of $\nabla\theta$ against FG at these points. The results for the area in Figure 33, are given in Table 4. The most significant change from the results of the previous method is the increased verification for positive and negative FG at 850 and 700 mb.

When the relation of FG to frontal movement was checked for all levels and for both temperatures fields, no correlation was observed. Centers of FG naturally moved in accordance with fronts, but gave no indication of future movement.

In summary, a review of the two tables shows that FG (especially negative FG) is best verified at 850 and 700 mb. In order to improve the relation of frontogenesis to changes in $\nabla\theta$, it was concluded that the non-conservative effects of the free atmosphere must be taken into consideration.

8. SHVF Analyses

The shear of the geostrophic wind component parallel to isentropes on a constant pressure surface (SHVF) (see equation 4) was obtained in units of 0.1 meters/sec/(100km). Figure 34 schematically shows the vector geostrophic wind component parallel to isentropes (VF), as indicated by arrows, in four shear-

producing situations. As with the other wind parameters, SHVF was computed at grid points for the five mandatory levels. Figure 36 shows the result over the North American area at 700 mb. Values of ± 8.0 meters/sec or approximately 16 knots/(100km) were the extremes observed, as found in the vicinity of GGθ fronts at 300 mb. The peak values decreased to ± 2.5 at the 1000-mb level, partially owing to decreased values of Vg.

In order to determine the relation between SHVF and GGθ fronts and baroclinic zones for the entire 63 x 63 grid, the following relationships were checked for both the processed and observed temperatures products. First, grid points within the baroclinic zone were categorized as to positive (cyclonic) or negative (anti-cyclonic) SHVF; secondly, all GGθ fronts were checked for algebraic sign of SHVF. Similarly, the USWB fronts were also checked at the only available constant pressure level, 850 mb.

Table 5 shows the results of the first method for 00Z and 12Z 20 August 1965. Only a slight overall tendency for grid points to experience positive SHVF rather than negative SHVF is noted. No large variation from this insignificant positive tendency exists at any level for either map time or with either temperature field.

The results of the second method are shown in Table 6. It is evident that there is a distinct tendency for fronts to lie mostly in positive SHVF at lower levels and predominately in negative SHVF at higher levels. This tendency shift from positive to

negative SHVF with height was observed at both times and with both temperatures, with only minor exceptions. Although it was not quantitatively investigated, it was noted qualitatively that the rear boundary of the baroclinic zone was characterized by positive SHVF at all levels. Table 7 shows an approximately equal distribution of USWB 850-mb fronts in areas of positive and negative SHVF, with a larger variation for the observed-temperature data. This distribution compares well with GGθ fronts.

The VF field was observed to be a combination of situations one and two of Figure 34. That is, maximum VF within the baroclinic zone produces negative SHVF at the warm-air boundary of baroclinic zones and positive SHVF at the cold-air boundary of baroclinic zones. VF maximum tends to shift in position from the vicinity of θ_2 to θ_1 with increasing height. Figure 35, showing VF plus a line of maximum VF and the baroclinic zones, and Figure 36, showing SHVF with respect to the GGθ baroclinic zones, illustrate this situation.

According to the common school of thought for fronts, the baroclinic zone is characterized by large positive shear. The SHVF patterns and the GGθ baroclinic zones miss this characterization by a small distance (less than one mesh length) at lower levels, but by a large distance (one half the width of the baroclinic zone) at higher levels. Maximum values of VF may be mislocated by as much as one half mesh length, due to the ability

of locating maximum values only at grid points, when in certain situations they should be more properly located between grid points. Although this lack of precision in locating VF maxima may have some effect on the SHVF-GGθ baroclinic zone relationship at lower levels, it is too small to have a significant effect at higher levels, where the baroclinic zone has a width of two to four mesh lengths. So, it is concluded that here negative SHVF is characteristic of upper-level baroclinic zones and fronts, while positive SHVF dominates low-level baroclinic zones and fronts.

To summarize, it is noted that the line of maximum VF within the baroclinic zone determines the peculiarities of the SHVF-baroclinic zone relationship for all levels tested. Also, the vertical variation of shear may be further evidence of dissimilar structure in fronts at low and high levels.

9. Final Conclusions and Recommendations

Except for the 1000-mb level, high latitudes, and the Asiatic continent, the processed temperature is considered to be a good approximation to the observed temperature, when moisture effects are considered. Since observed temperatures suppress intensity of fronts over water surfaces at lower levels and is a poor front indicator at 1000 mb, it is considered inferior to GGθp at lower levels. At the three upper levels (700, 500, and 300 mb), GGθp and GGθo are comparable. Perhaps a test using observed virtual temperature is now in order, as this would allow a better evaluation of the FNWF virtual temperatures products.

Of the three wind parameters studied, VNF manifests itself as being the most promising, especially at 850 mb,using processed temperatures. Its ability to indicate instantaneous front movement and its time consistency is suggestive of incorporating VNF into the numerical frontal analysis systems.

Due to the numerous non-conservative effects present in the atmosphere, of which none were taken into account in determining frontogenesis, FG was found to be of limited value as an indicator of changes in intensity of baroclinic zones.

Before stating positively that fronts lie predominately, although not completely, in positive SHVF at lower levels and primarily in negative SHVF at higher levels, it is recommended that SHVF be recomputed using smaller grid lengths and/or utilizing a smaller computation interval.

It would be improper to assume that the results of this study are applicable in general, since only two observation times of a summer date were used. Therefore a similar study for a winter date would be beneficial in establishing the generality of the results obtained.

10. Acknowledgements

The writer's grateful thanks are due to Associate Professor Robert J. Renard for his advice and support in preparing this paper. A special thanks is also given to Mr. Leo Clarke of the U. S. Navy Fleet Numerical Weather Facility for programming the

various parameters and for production of the necessary data. Thanks are also in order for the members of the U. S. Navy Fleet Numerical Weather Facility and U. S. Naval Postgraduate School, who assisted in various capacities.

BIBLIOGRAPHY

1. Clarke, L. C. and R. J. Renard. The U. S. Navy frontal analysis scheme: further development and a limited evaluation. Publication pending, Journal of Applied Meteorology, 1966.

2. Duthie, W. D. Notes on the analysis of weather charts. Unpublished manuscript, Dept. of Meteorology and Oceanography, NPGS, 1964.

3. Ferrentino, P. S. The error analysis of Fleet Numerical Weather Facility temperature analyses. Unpublished manuscript, Dept. of Meteorology and Oceanography, NPGS, October, 1965.

4. Hamrick, J. M. A frontal comparison between a hand-analyzed product and a numerical product. Unpublished manuscript, Dept. of Meteorology and Oceanography, NPGS, October, 1965.

5. Holl, M. H., J. P. Bibbo and J. R. Clark. Linear transforms for state parameter structure. Meteorology International, Inc. Tech. Memo. No. 1, 1963.

6. Petterssen, S. Weather Analysis and Forecasting, 2nd ed., v. 1, McGraw-Hill, 1956: 201-202.

7. Reed, R. J. A study of a characteristic type of upper-level frontogenesis. Journal of Meteorology, v. 12, 1954: 226-237.

8. Renard, R. J. and L. C. Clarke. Experiments in numerical objective frontal analysis. Monthly Weather Review, v. 93, 1965: 547-556.

9. Sanders, F. A survey of frontal zones in the middle and upper troposphere. Presented at the 45th Annual Meeting of the American Meteorological Society, New York City, January, 1965.

TABLE 1

FNWF PROCESSED TEMP MINUS OBSERVED TEMP: 00Z 20 AUG 1965

	0.0 to +0.9	0.0 to -0.9	+1.0 to +2.9	-1.0 to -2.9	+3.0 to +5.9	-3.0 to -5.9	>+6.0	<-6.0
300 mb								
South	30	13	45	6	5	1		
Central	31	24	26	16	1	2		
North	22	25	20	25	2	6		
500 mb								
South	47	25	16	8	3	1		
Central	42	35	15	6	1	1		
North	36	32	18	11	3			
700 mb								
South	43	14	41		2			
Central	29	16	46	5.5	2	1	0.5	
North	29	22	31	2	5.5	0.5		
850 mb								
South	17	12	54	6	9.5	1	0.5	
Central	20	13	47	8.5	8.5	3		
North	29	22	33	11	3	2		
1000 mb								
South	14	7	42	4	23	1	9	
Central	11	11	23	9	23	4	17	2
North	17	13	26	12	18.5	4.5	9	

TABLE 2

FNWF PROCESSED TEMP MINUS OBSERVED TEMP: 00Z 20 AUG 1965

	0.0 to +0.9	0.0 to -0.9	+1.0 to +2.9	-1.0 to -2.9	+3.0 to +5.9	-3.0 to -5.9	>+6.0	<-6.0
300 mb								
N.America	22	26	36	12.5	1	2.5		
Pacific	38	23	28	8	2.5	0.5		
Asia	24	20	27	17	7	5		
Europe	28	19	39	9	4	1		
Atlantic	29	18	36	14		3		
500 mb								
N.America	43	27	21	9				
Pacific	53	27	14	4.5	1.5			
Asia	31	32	17	18		2		
Europe	40	26	21	6	7			
Atlantic	44	38	11	7				
700 mb								
N.America	34	13	47	3	3			
Pacific	38	24	30	6	1	1		
Asia	28	13	48	6	4	0.5	0.5	
Europe	37	21	30	9	2	1		
Atlantic	39	6	49	2		4		
850 mb								
N.America	18	12	54	8	6.5	1.5		
Pacific	19	6	63	3	8.5	0.5		
Asia	16	19	35	18	7.5	4.5		
Europe	31	27	30	7.5	3.0	1.5		
Atlantic	14	8	64	11	1.5	1.5		
1000 mb								
N.America	14	8	34	6	26	1	11	
Pacific	23	14	41	9	7.5	3.5	1	1
Asia	6	27	21	7	24	5	27	3
Europe	11	8	26	4.5	31	2.5	17	
Atlantic	12	12	39	8	26	1	2	

TABLE 3

	AREA OF POSITIVE FG		AREA OF NEGATIVE FG	
	AGREES WITH $\nabla\theta$ CHANGE (in %)	DISAGREES WITH $\nabla\theta$ CHANGE (in %)	AGREES WITH $\nabla\theta$ CHANGE (in %)	DISAGREES WITH $\nabla\theta$ CHANGE (in %)
USING PROCESSED TEMPERATURE				
1000 mb	44	56	57	43
850 mb	55	45	89	11
700 mb	63	37	80	20
500 mb	52	48	57	43
USING OBSERVED TEMPERATURE				
850 mb	54	46	61	39
500 mb	52	48	34	66

TABLE 4

USING PROCESSED TEMPERATURE	AREA OF POSITIVE FG		AREA OF NEGATIVE FG	
	AGREES WITH $\nabla\theta$ CHANGE (# pts)	DISAGREES WITH $\nabla\theta$ CHANGE (# pts)	AGREES WITH $\nabla\theta$ CHANGE (# pts)	DISAGREES WITH $\nabla\theta$ CHANGE (# pts)
1000 mb		2	4	2
850 mb	7	2		
700 mb	2		2	
500 mb	3	4	2	1

TABLE 5

SHVF

	0000Z		1200Z	
	POSITIVE (in %)	NEGATIVE (in %)	POSITIVE (in %)	NEGATIVE (in %)
PROCESSED TEMPERATURE				
1000 mb	57	43	58	42
850 mb	57	43	54	46
700 mb	57	43	46	54
500 mb	55	45	49.5	50.5
300 mb	51	49	48	52
OBSERVED TEMPERATURE				
1000 mb	48	52		
850 mb	55	45	52	48
700 mb	52	48		
500 mb	56	44	44	56
300 mb	49	51		

TABLE 6

SHVF

	0000Z		1200Z	
	POSITIVE (in %)	NEGATIVE (in %)	POSITIVE (in %)	NEGATIVE (in %)
PROCESSED TEMPERATURE				
1000 mb	79	21	60	40
850 mb	52	48	54	46
700 mb	35	65	22	78
500 mb	21	79	12	88
300 mb	14	86	02	98
OBSERVED TEMPERATURE				
1000 mb	58	42		
850 mb	59	41	52	48
700 mb	26	74		
500 mb	17	83	15	85
300 mb	07	93		

TABLE 7

850 mb SHVF

	PROCESSED TEMPERATURE		OBSERVED TEMPERATURE	
	POSITIVE (in %)	NEGATIVE (in %)	POSITIVE (in %)	NEGATIVE (in %)
00Z	50	50	40	60
12Z	58	42	62	38

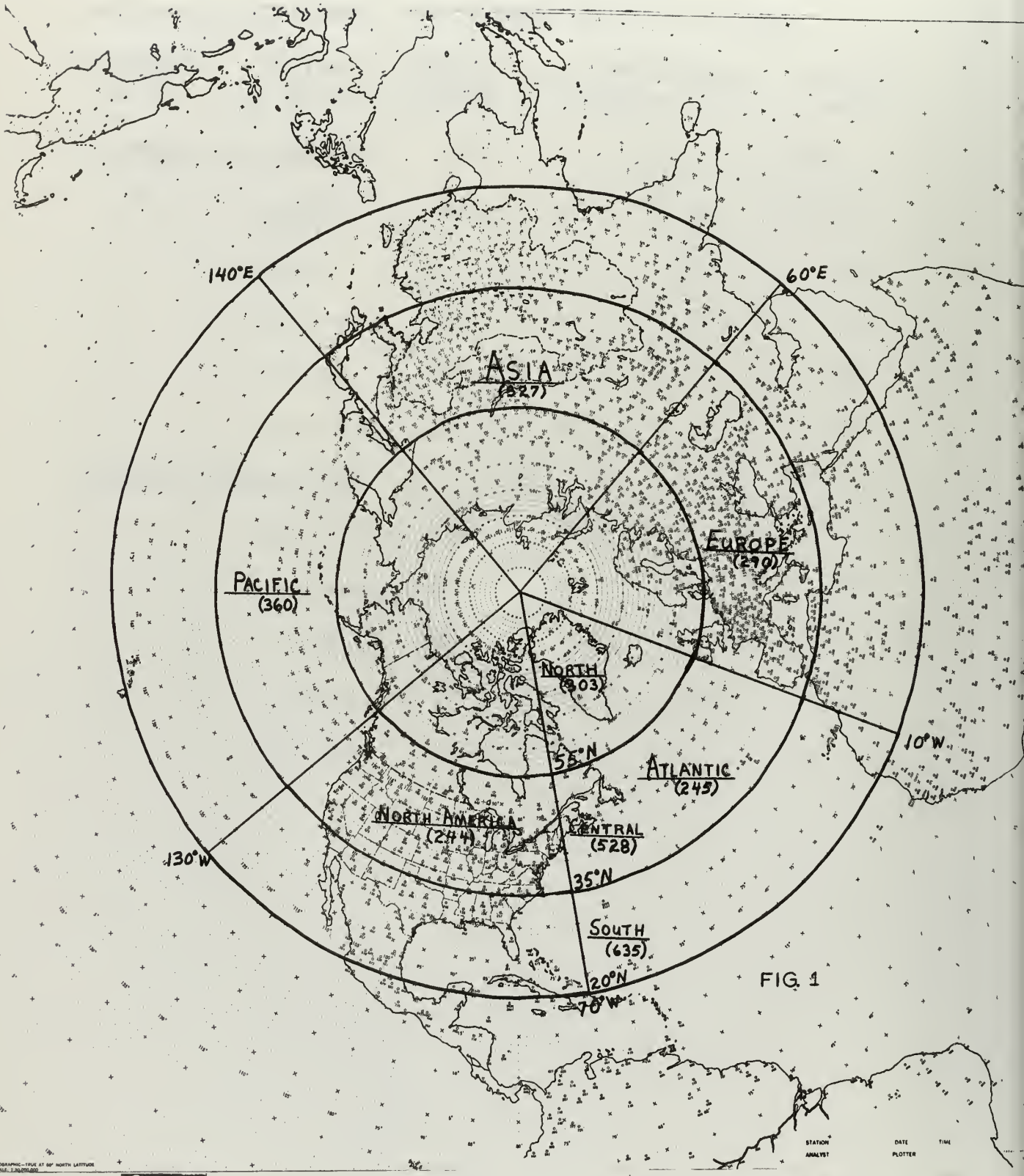
140°E
60°E
ASIA
(827)
EUROPE
(270)
PACIFIC
(360)
NORTH
(503)
55°N
ATLANTIC
(245)
NORTH AMERICA
(244)
CENTRAL
(528)
130°W
35°N
SOUTH
(635)
20°N
70°W
10°W
STEREOGRAPHIC — TRUE AT 60° NORTH LATITUDE
STATION
ANALYST
DATE
PLOTTER
TIME

FIG. 1

FIG. 2

FIG. 3

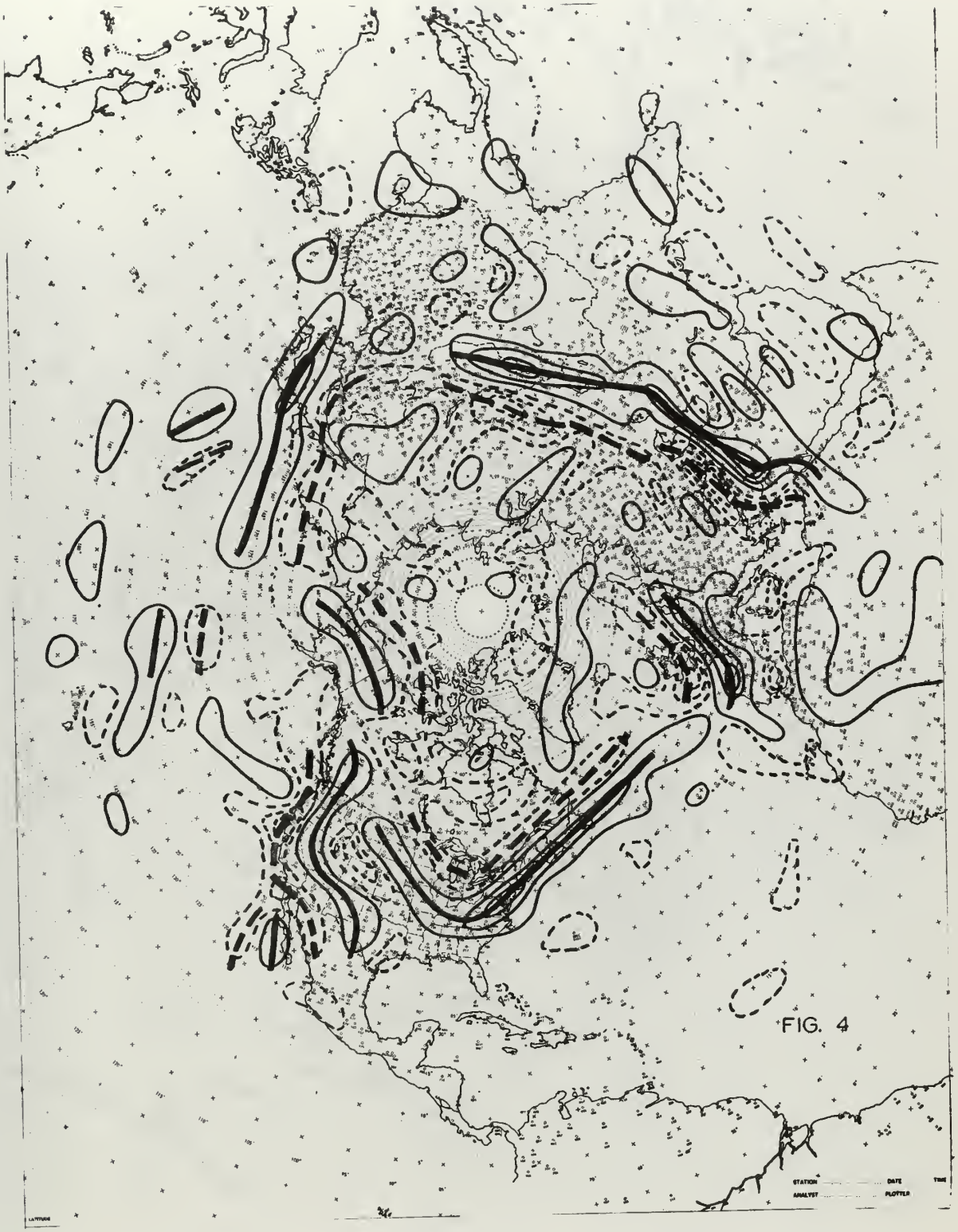

FIG. 4

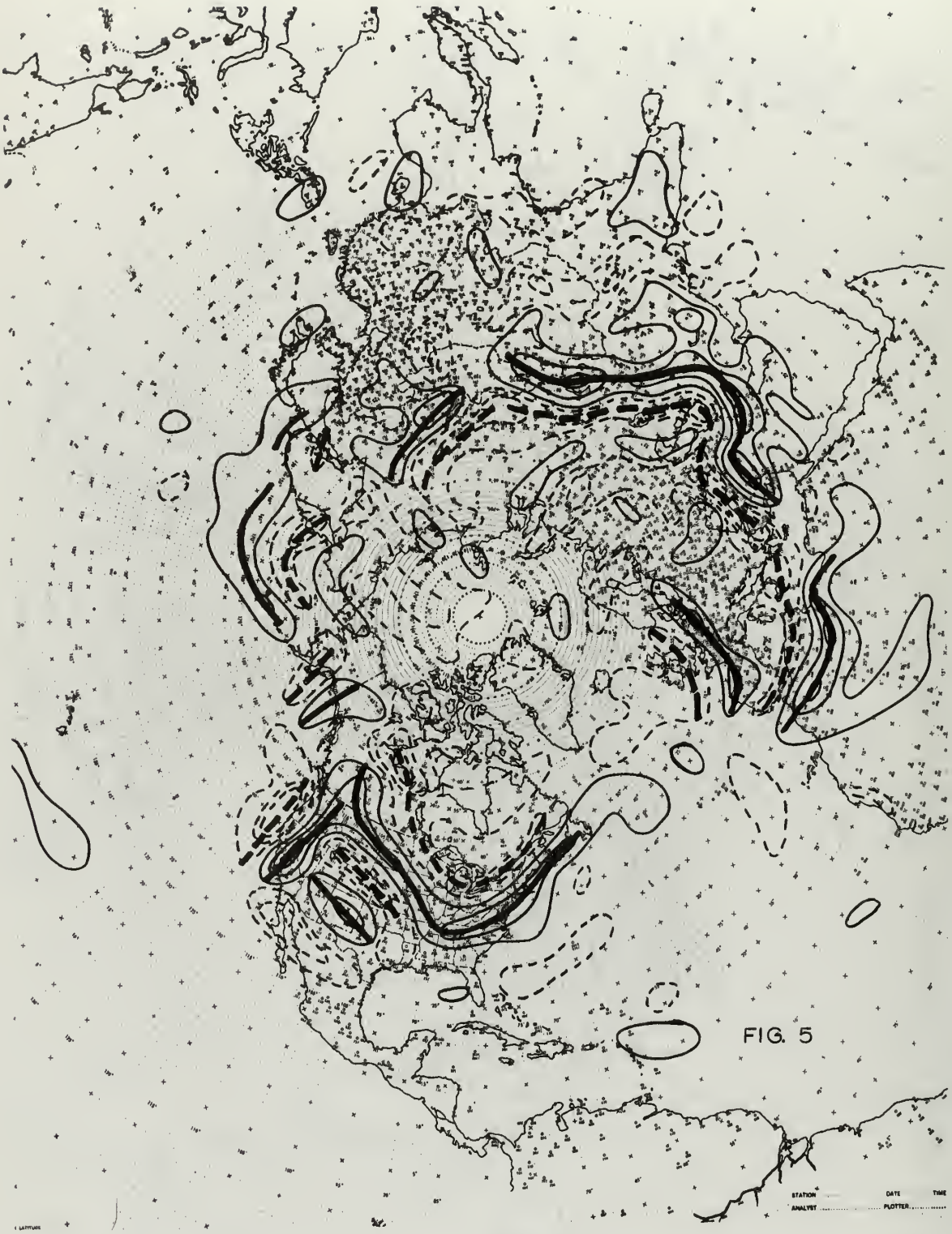

FIG. 5

FIG. 6

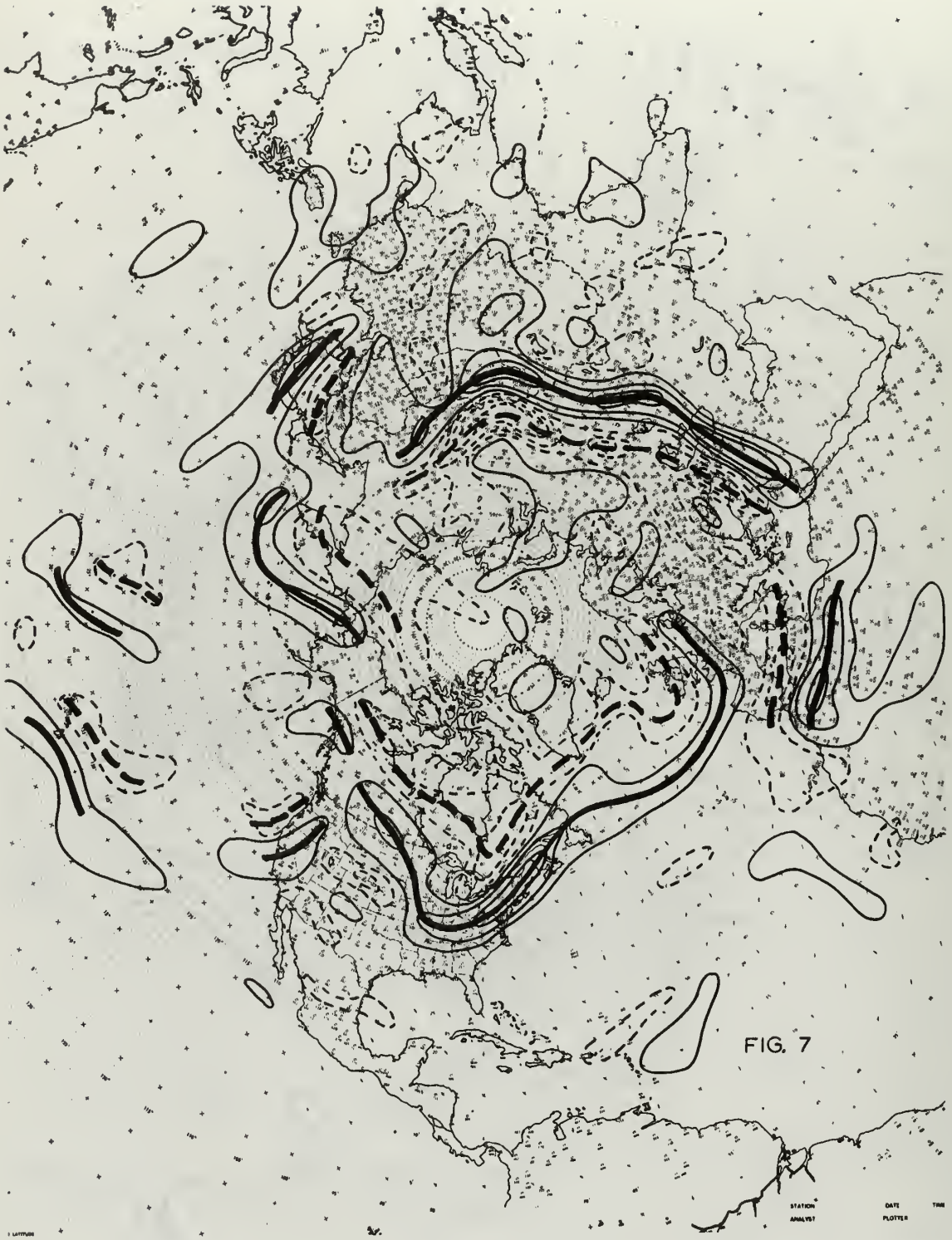

FIG. 7

FIG. 8

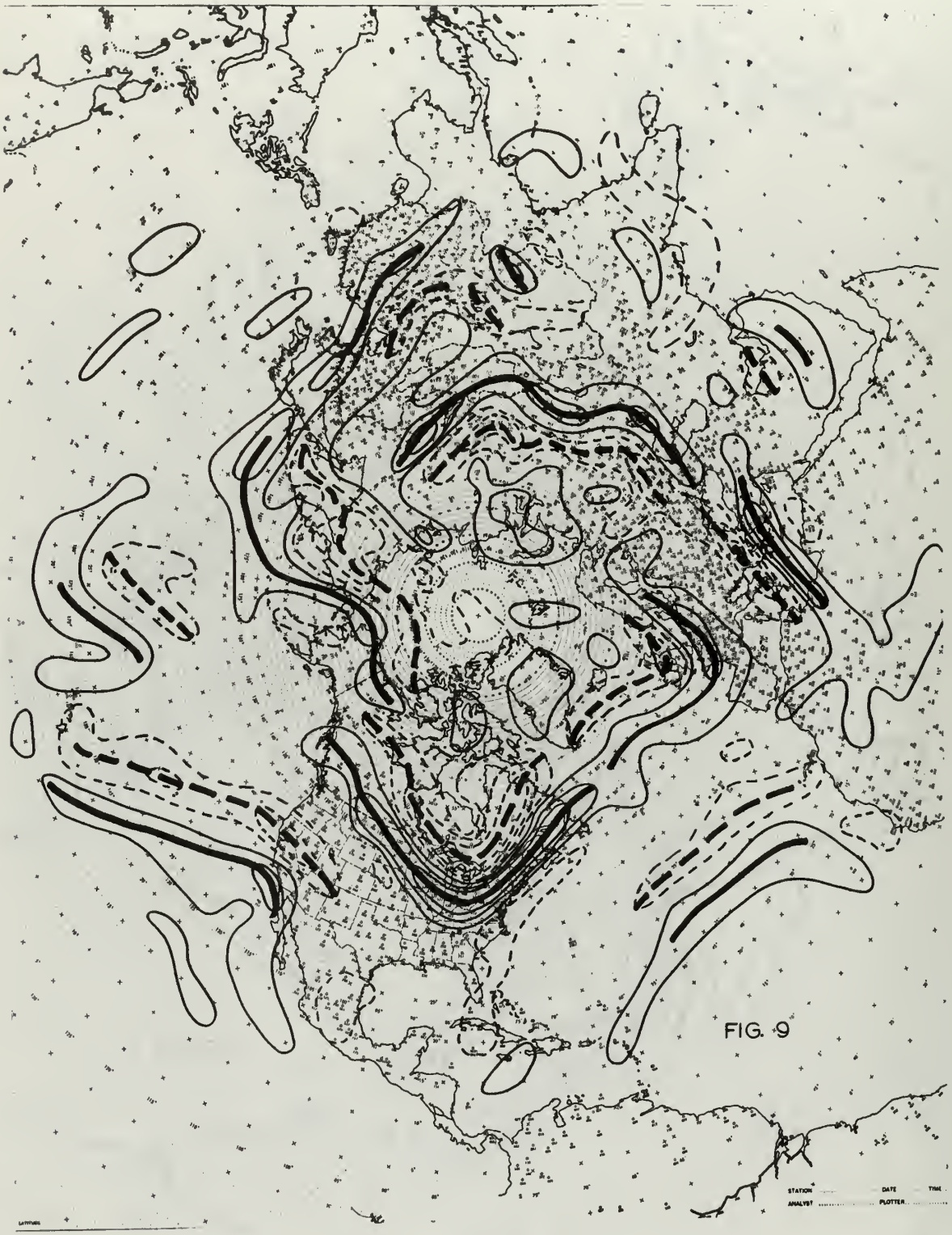

FIG. 9

FIG. 10

FIG. 11

FIG. 12

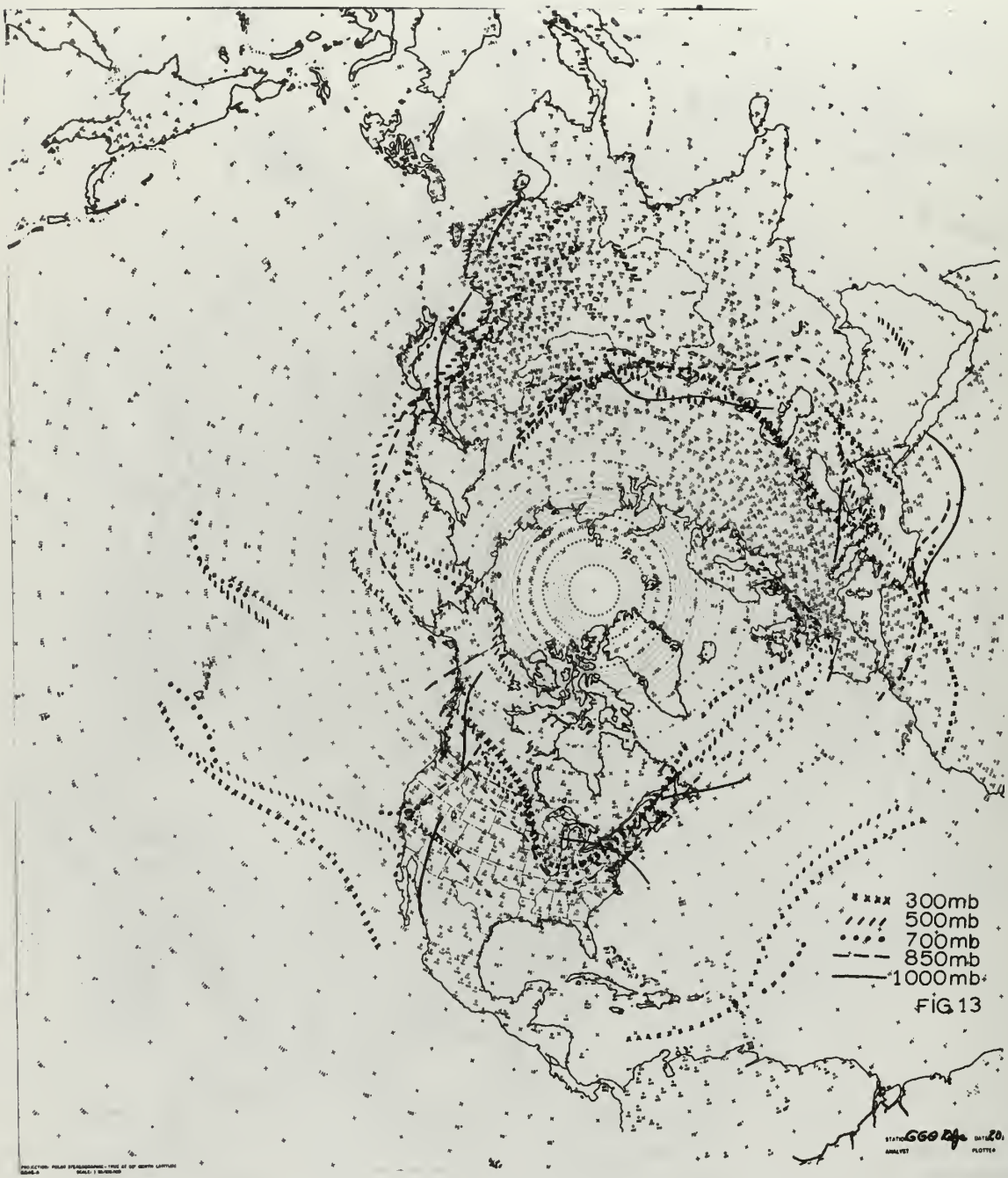

FIG 13

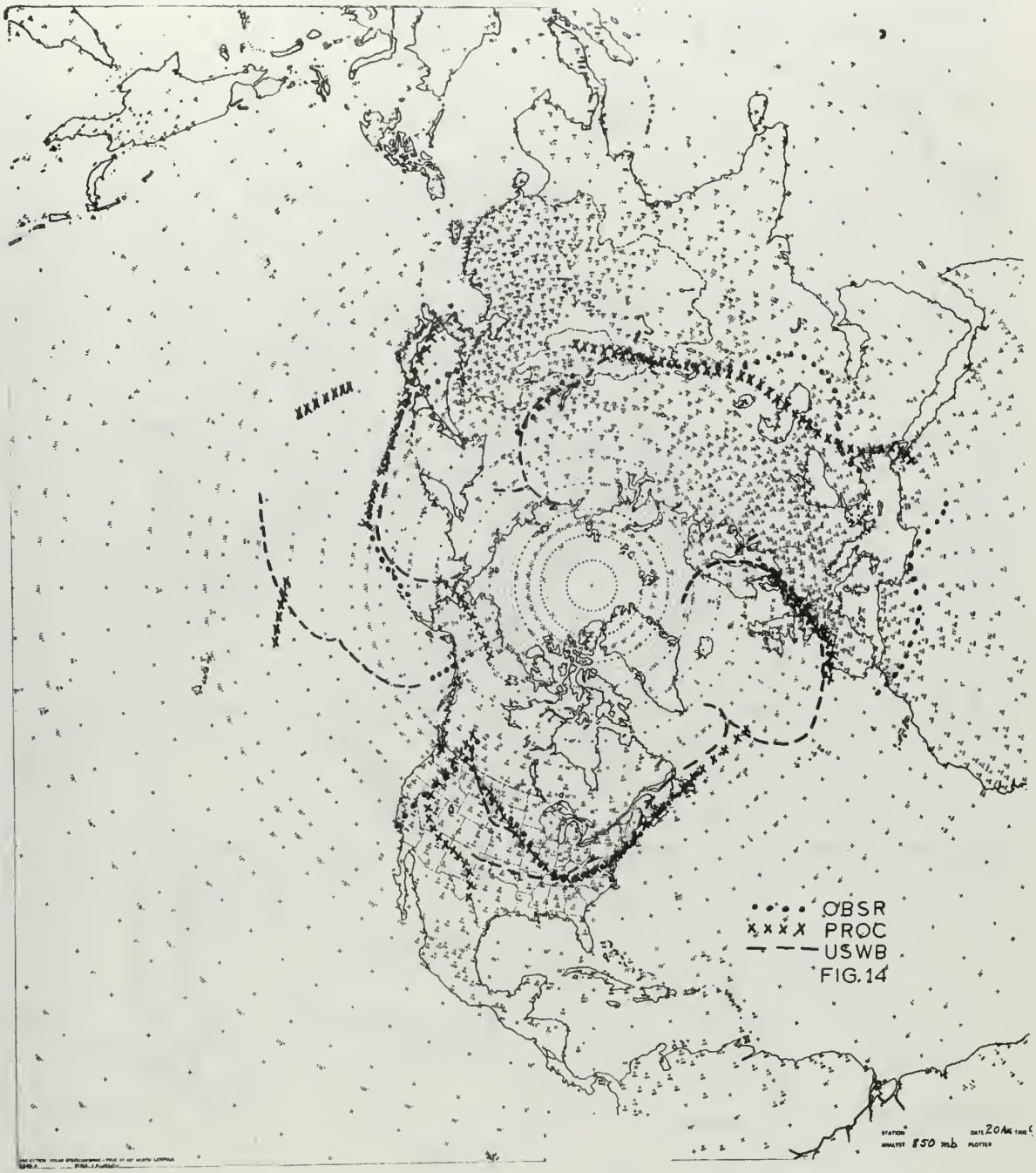
OBSR
PROC
USWB
FIG. 14

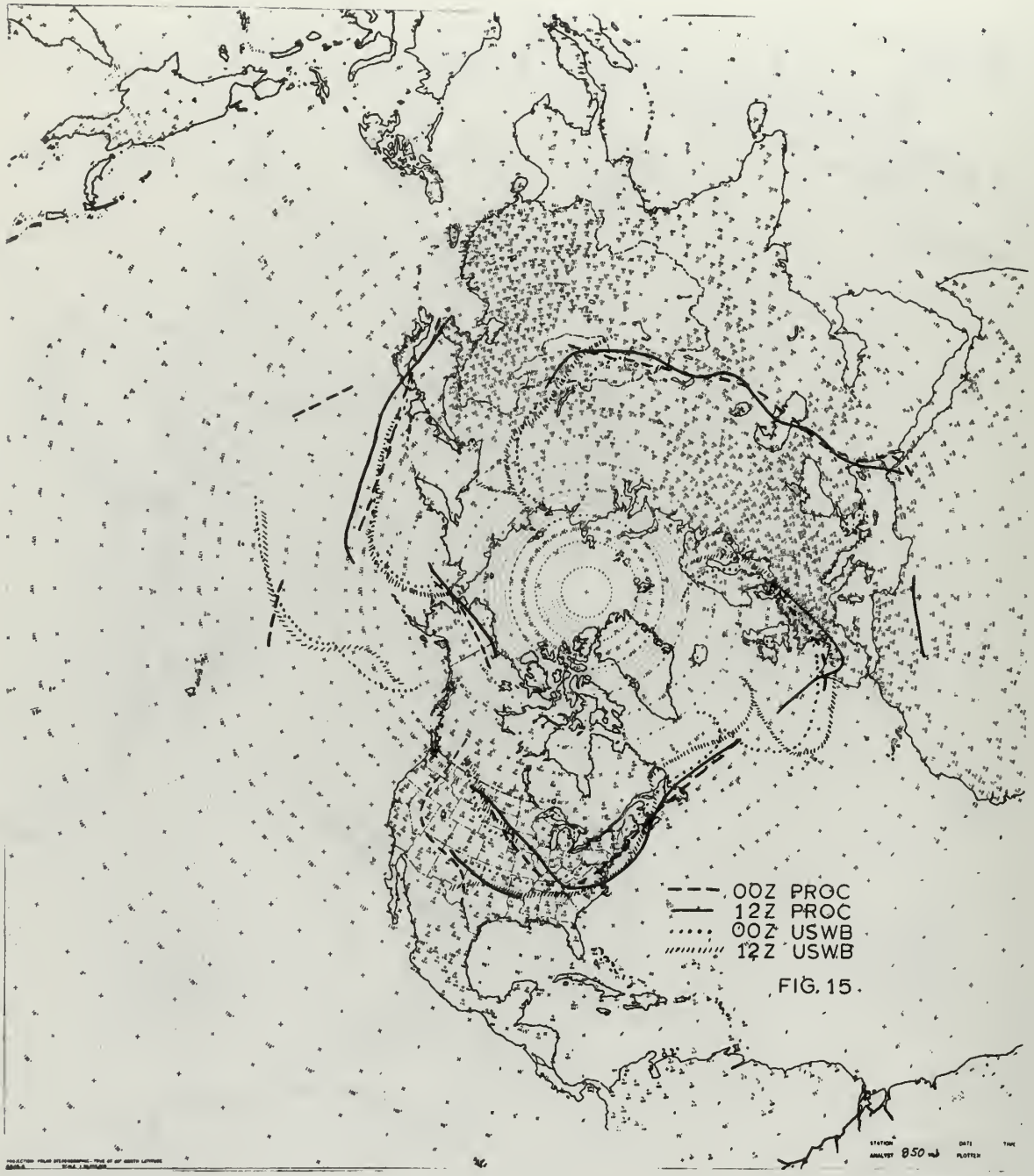
00Z PROC
12Z PROC
00Z USWB
12Z USWB
FIG. 15.

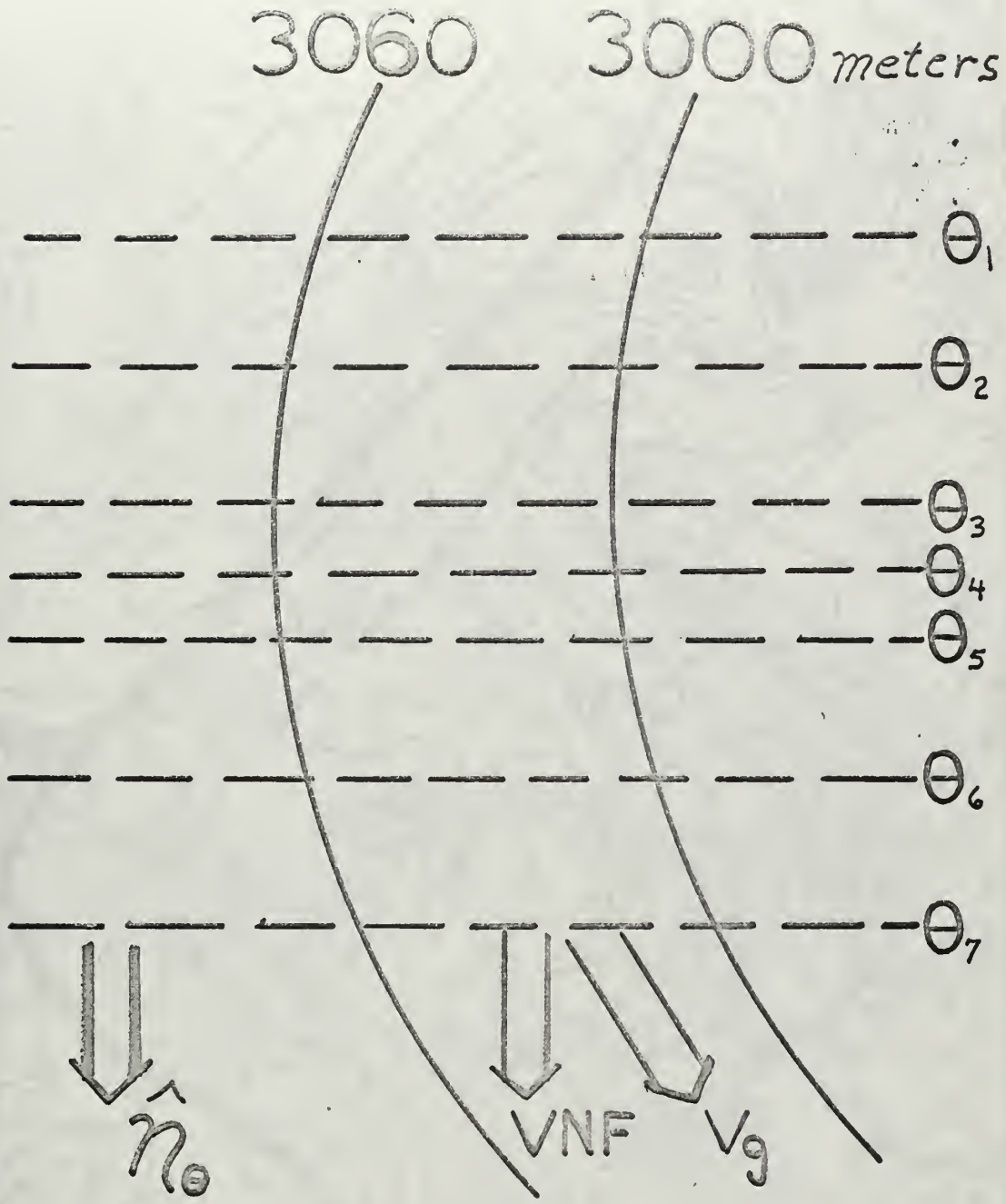
3060
3000
meters
θ_1
θ_2
θ_3
θ_4
θ_5
θ_6
θ_7
$\hat{n}_\theta$
VNF
V_g

FIG. 16

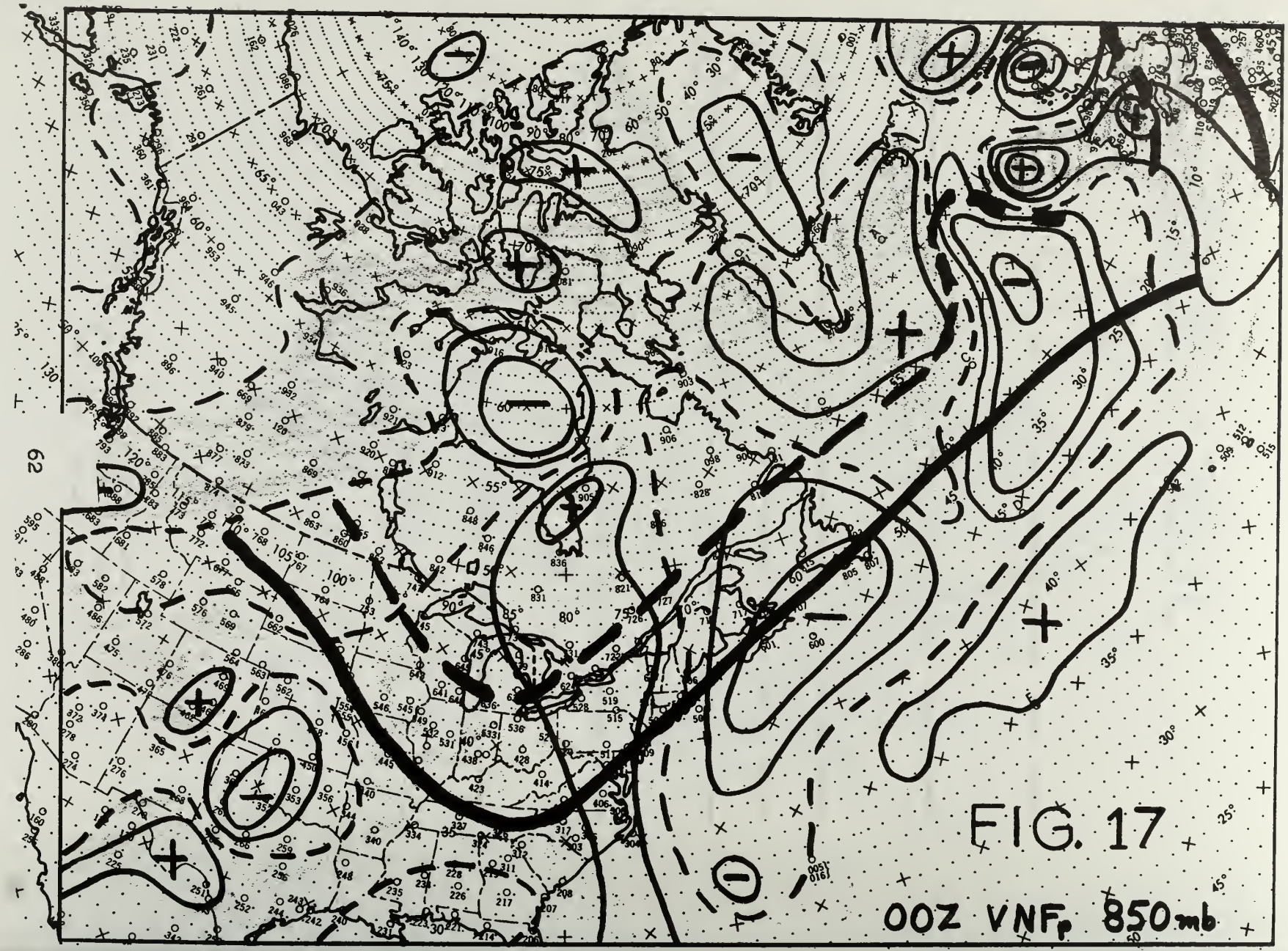

FIG. 17

00Z VNFp 850mb

FIG. 18

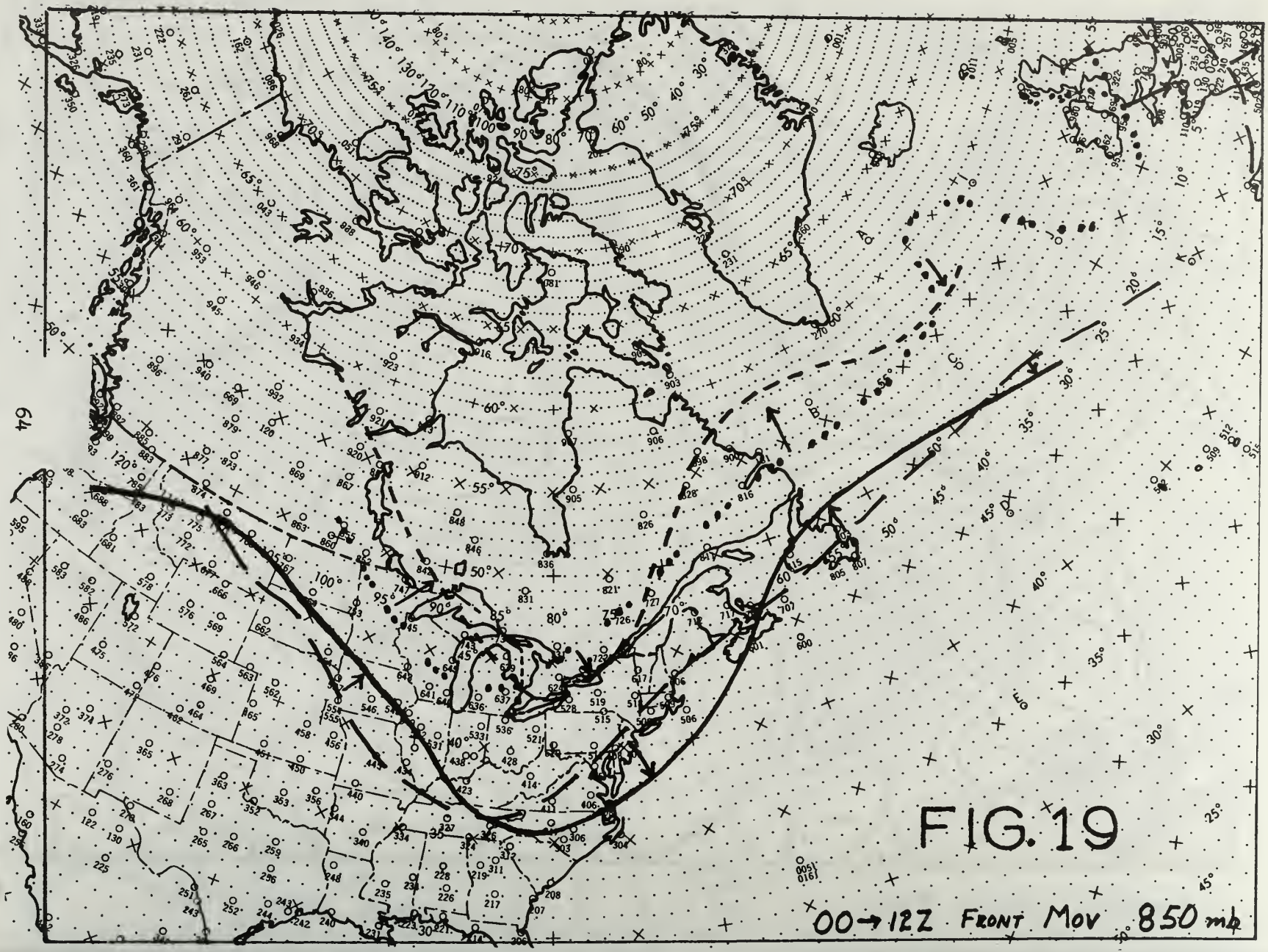

FIG. 19

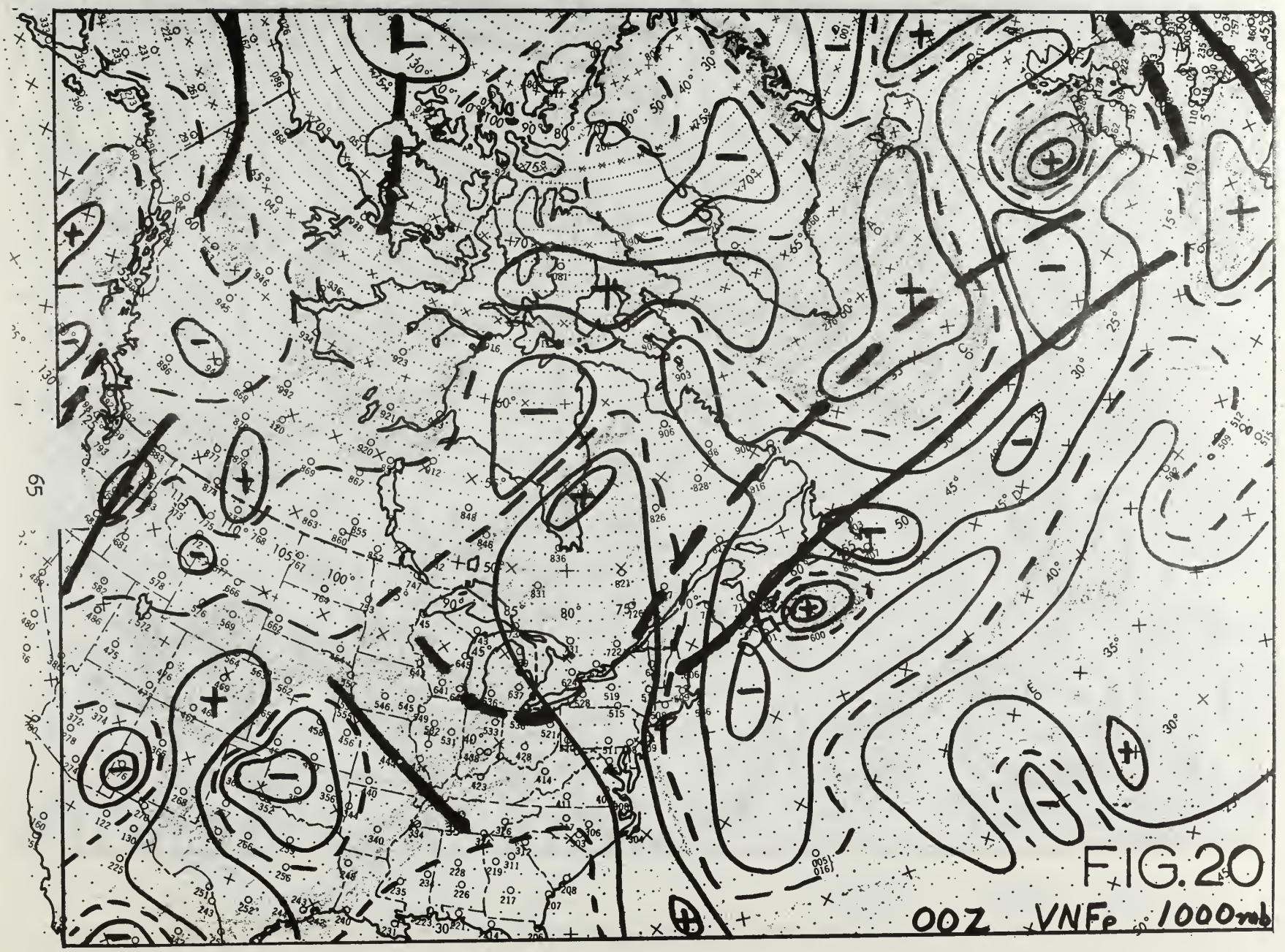

FIG. 20

FIG 21
12 Z VNFP 1000 mb

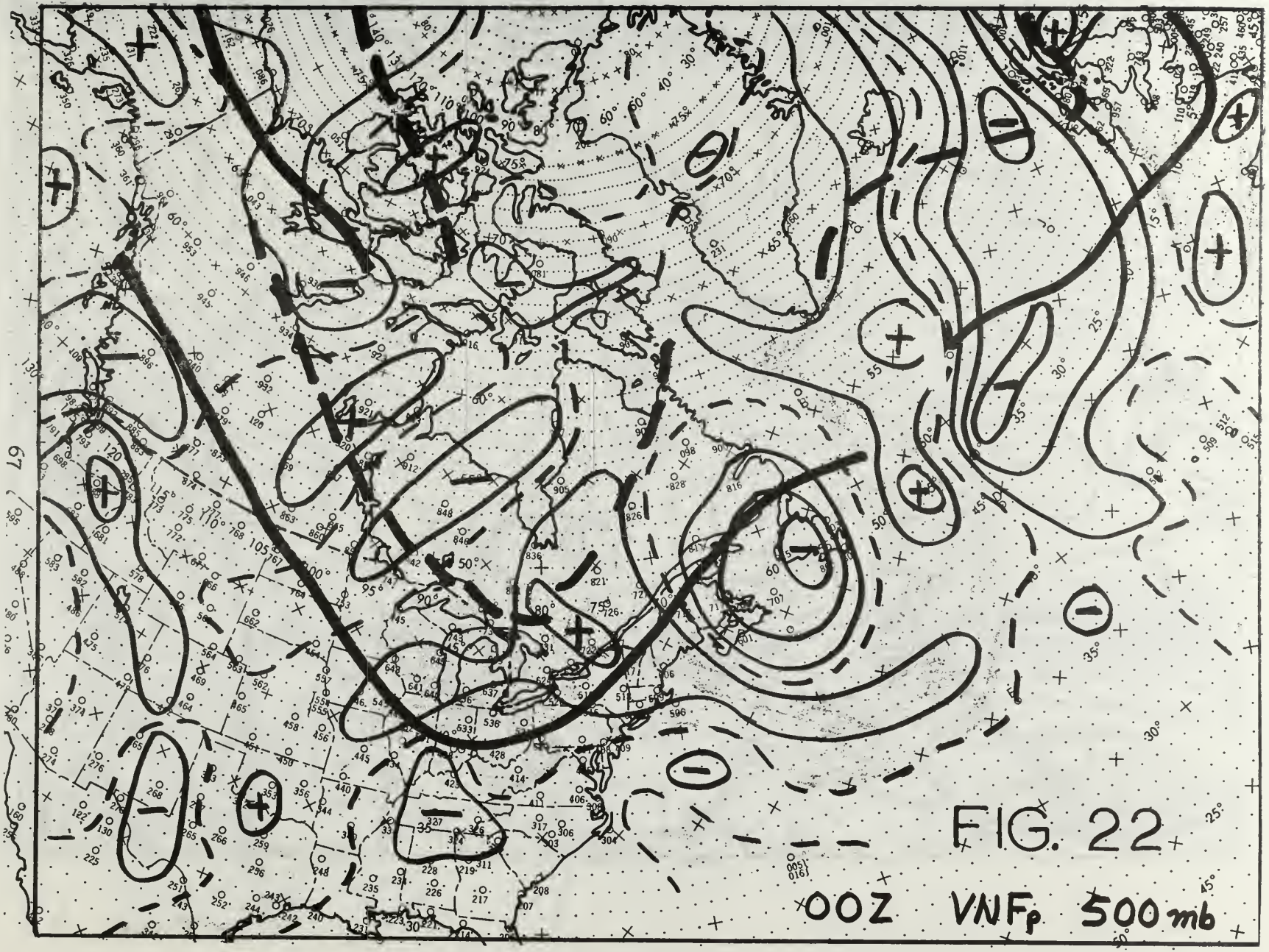

FIG. 22

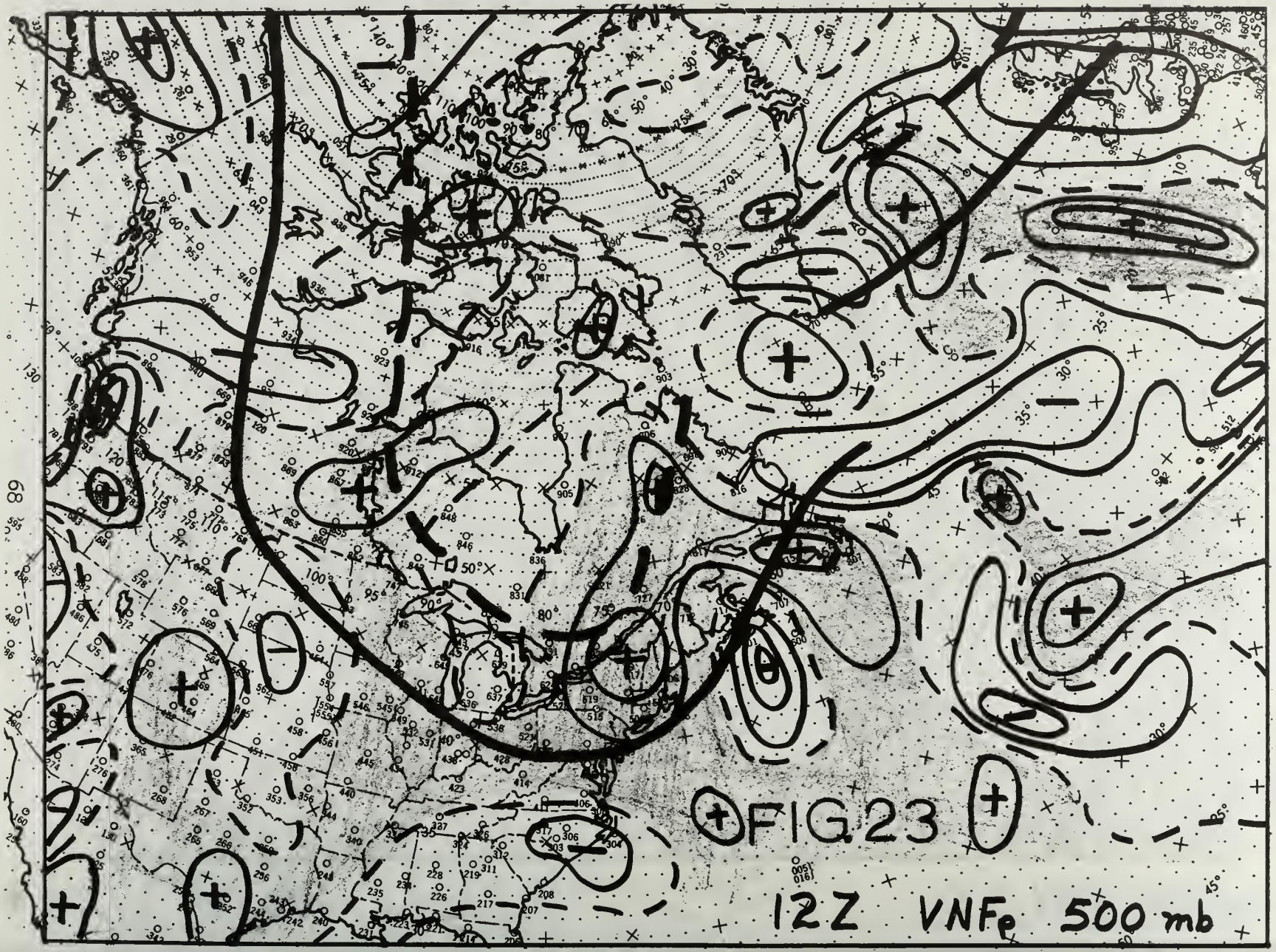
FIG 23
12Z VNFe 500 mb

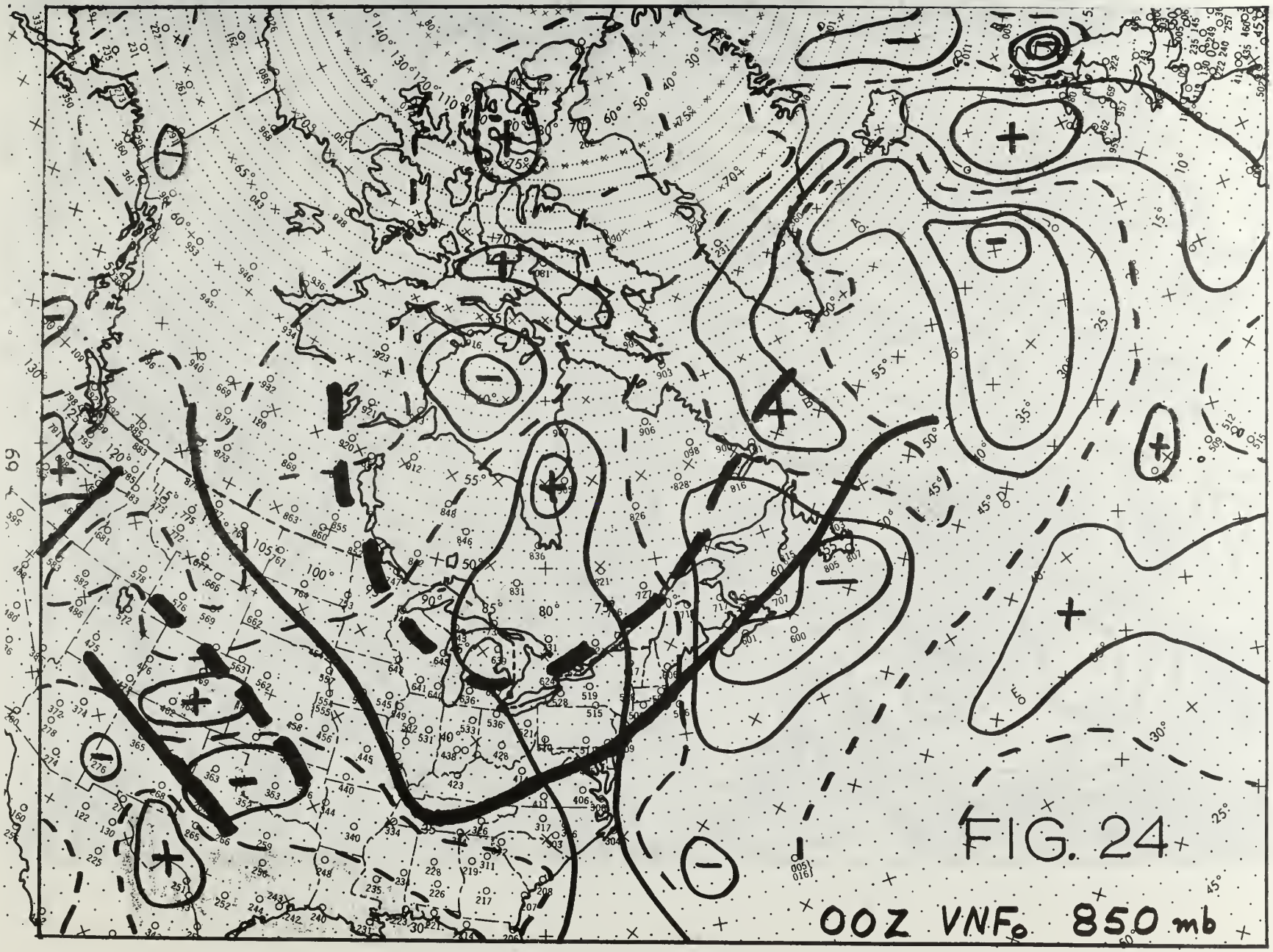
FIG. 24
00Z VNF. 850 mb

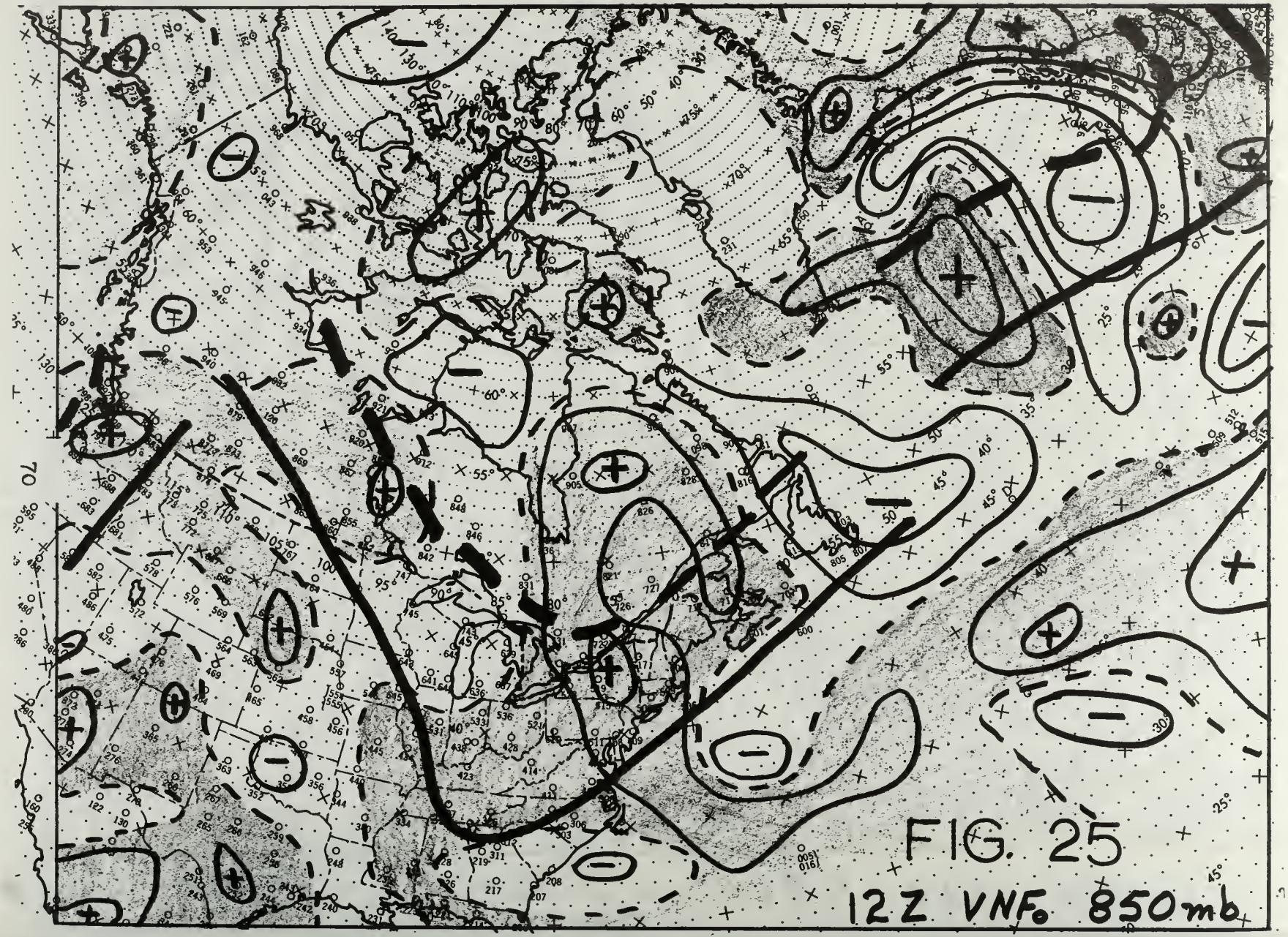

FIG. 25

12Z VNF 850mb

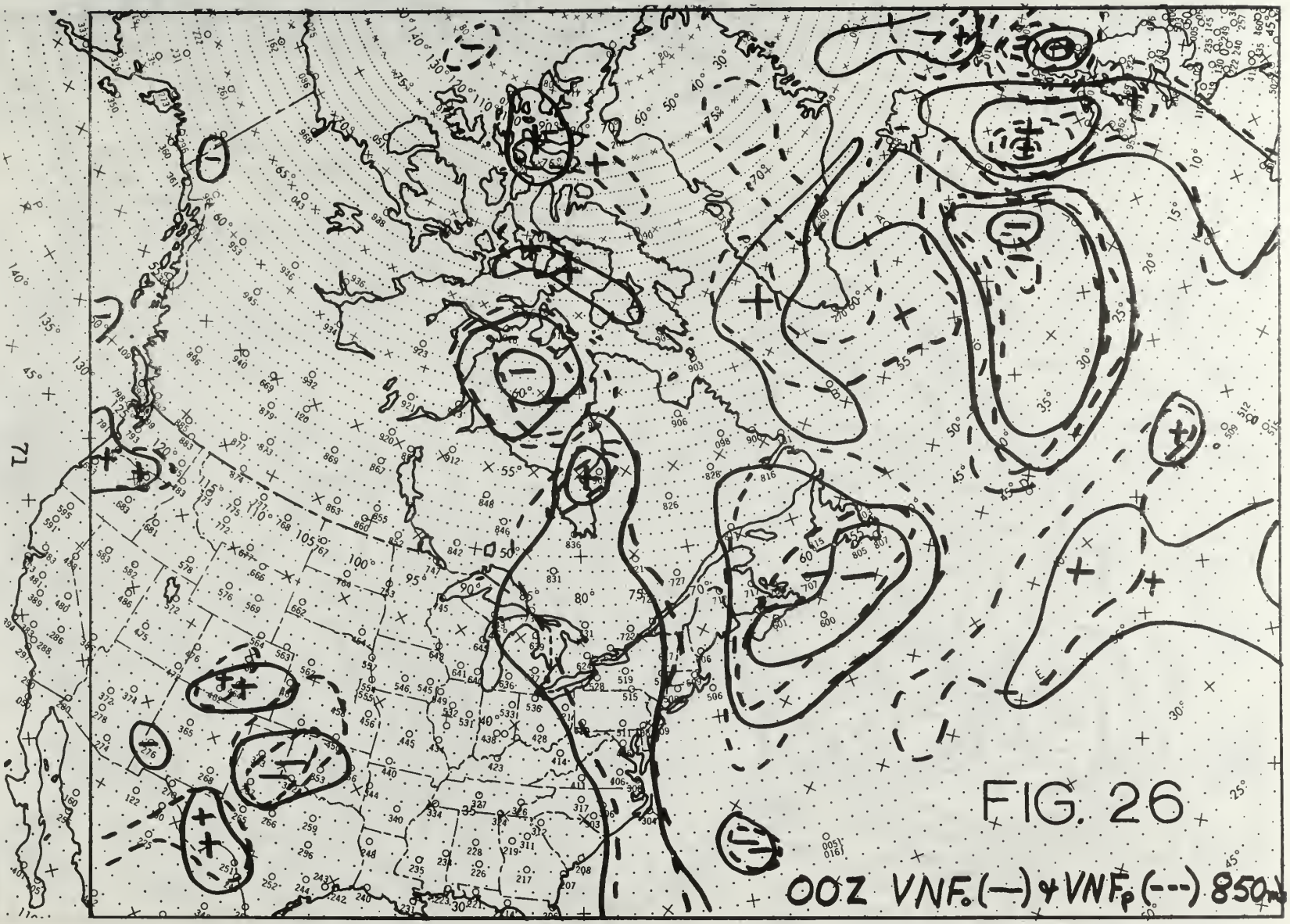

FIG. 26

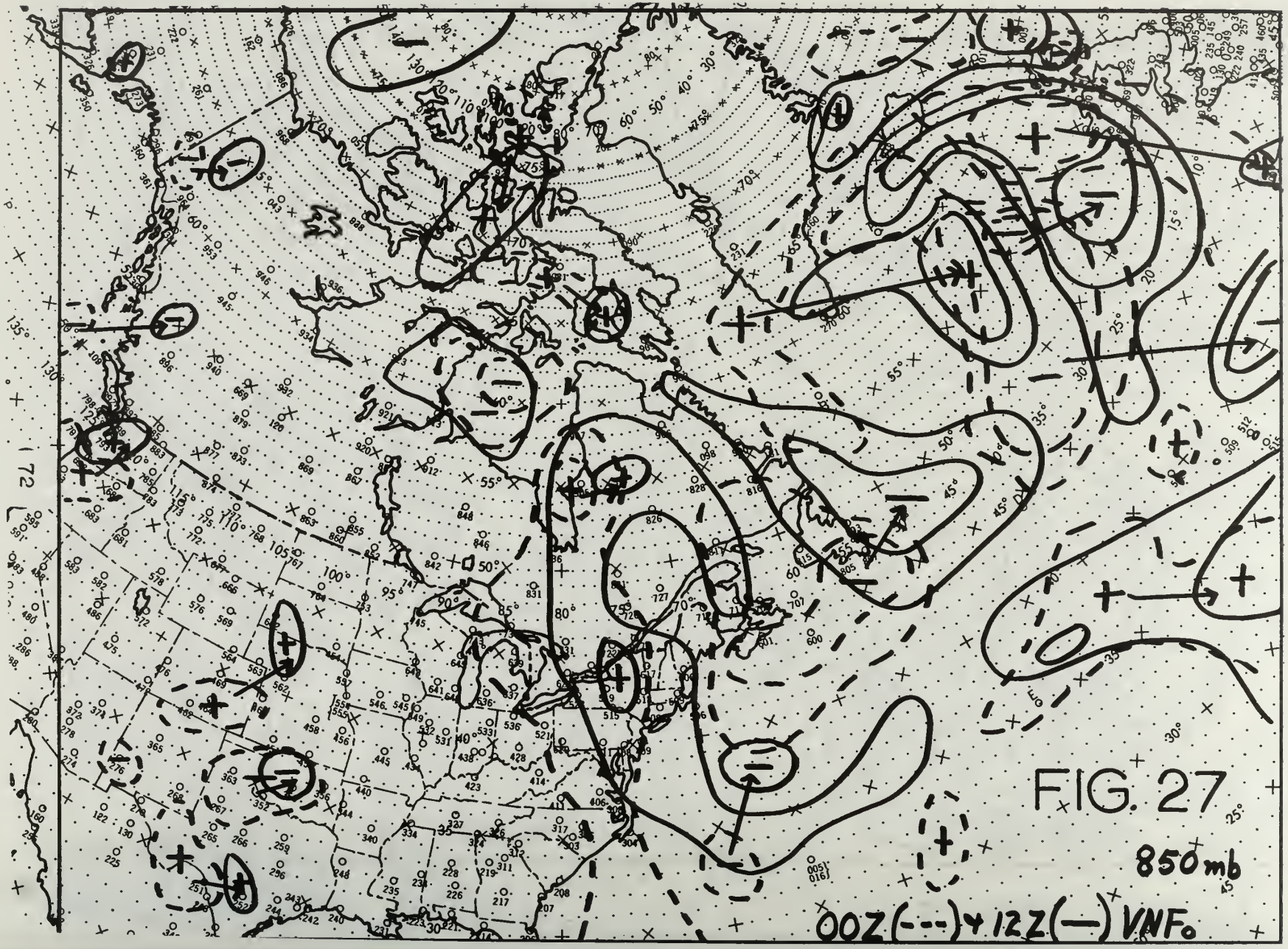
FIG. 27
850mb
00Z(---)+12Z(—) VNFo

FIG. 28
USWB FRONT Vk. VNEP
00Z 850 mb

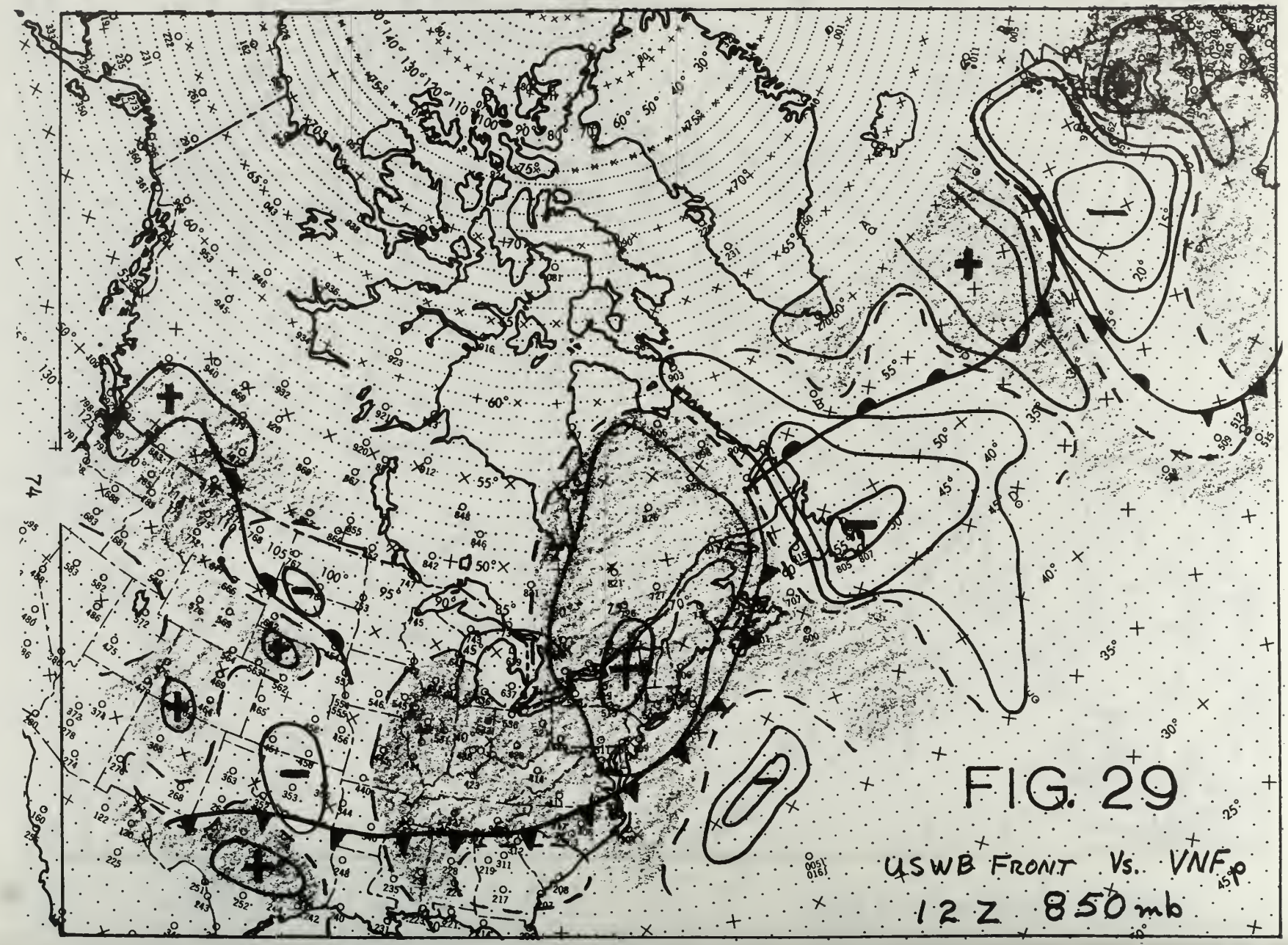

FIG. 29

USWB FRONT Vs. VNFP

12Z 850 mb

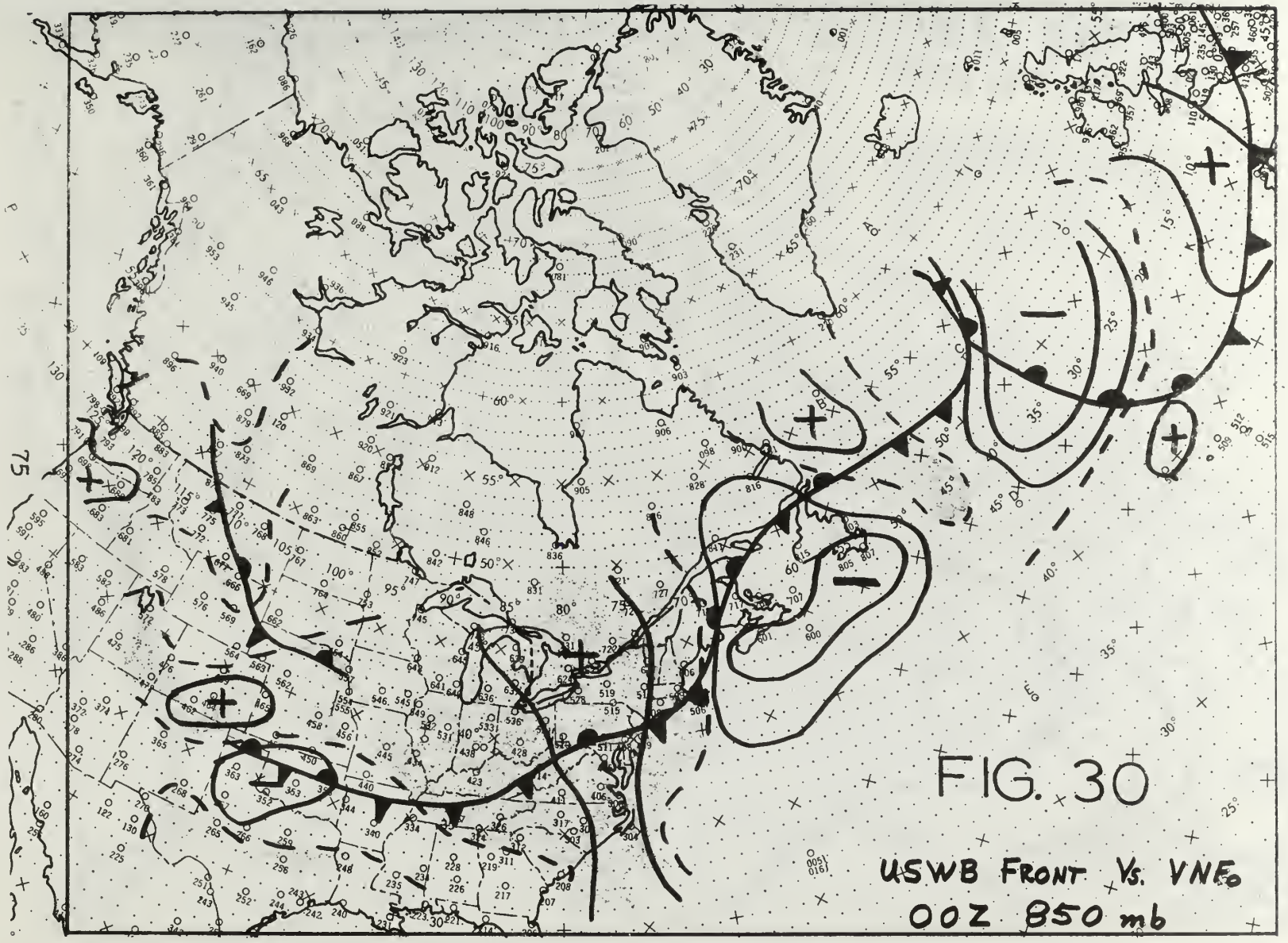

FIG. 30

USWB FRONT Vs. VNEO
00Z 850 mb

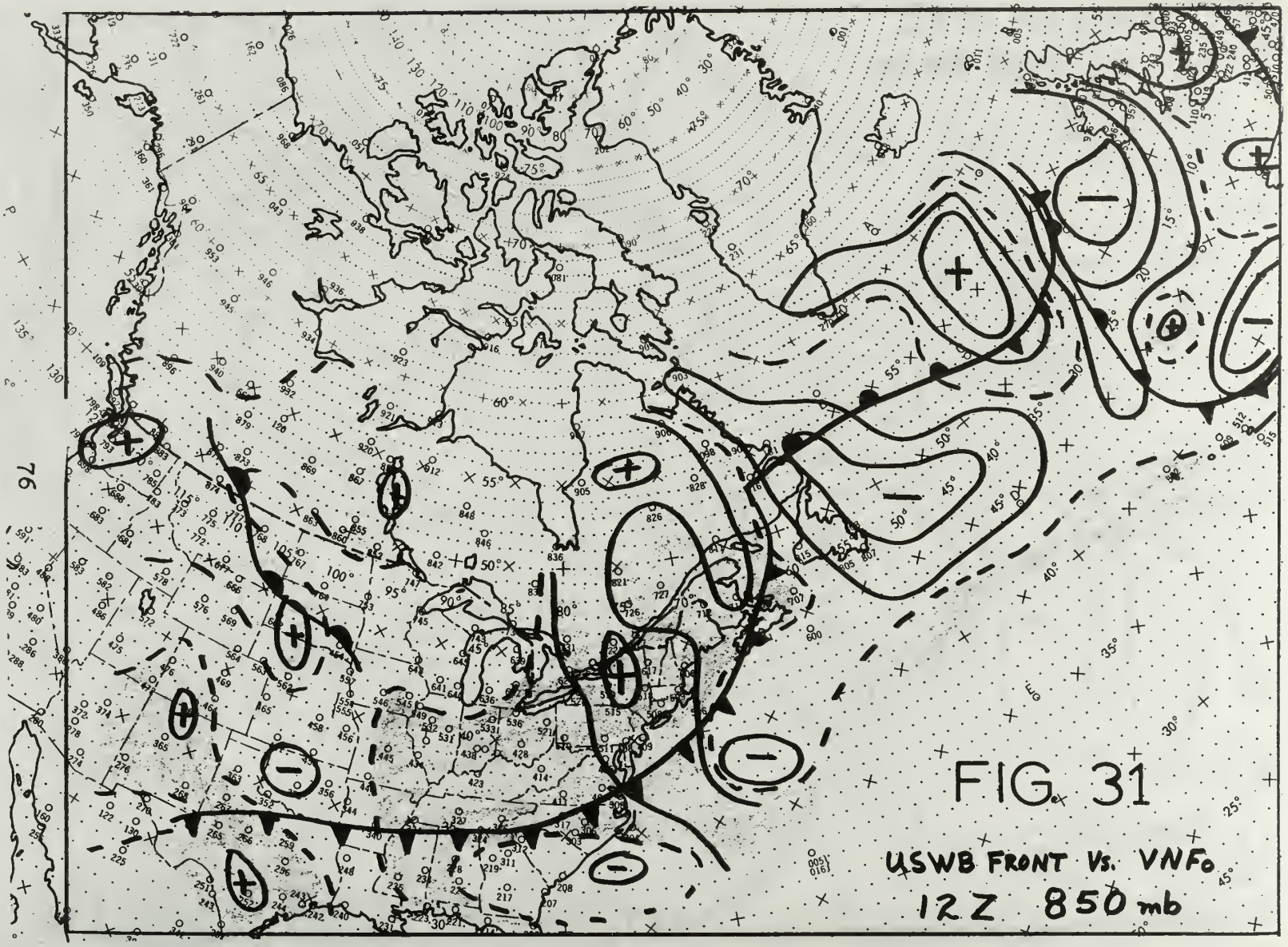

FIG. 31

USWB FRONT Vs. VNFo

12Z 850 mb

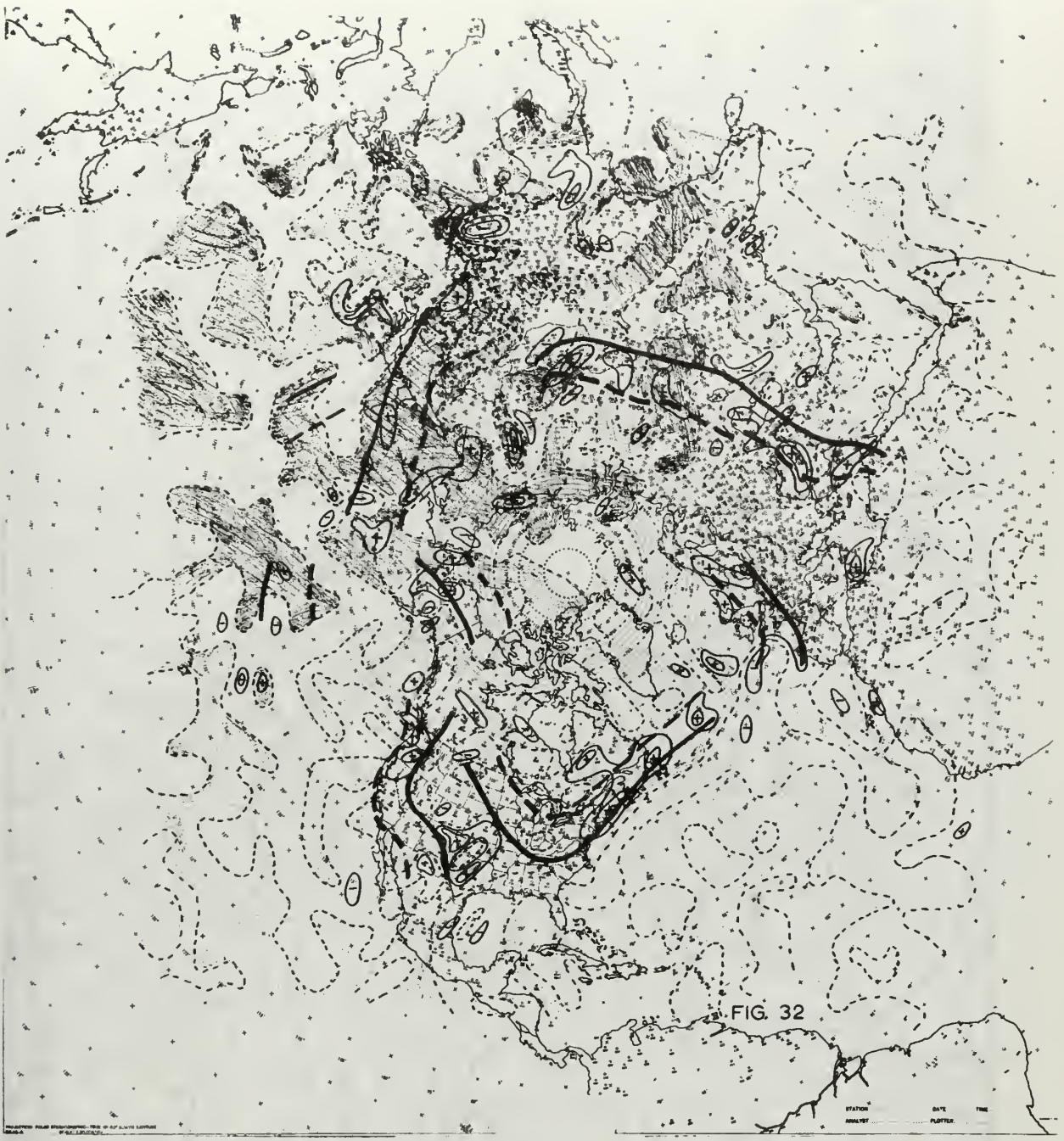

FIG. 32

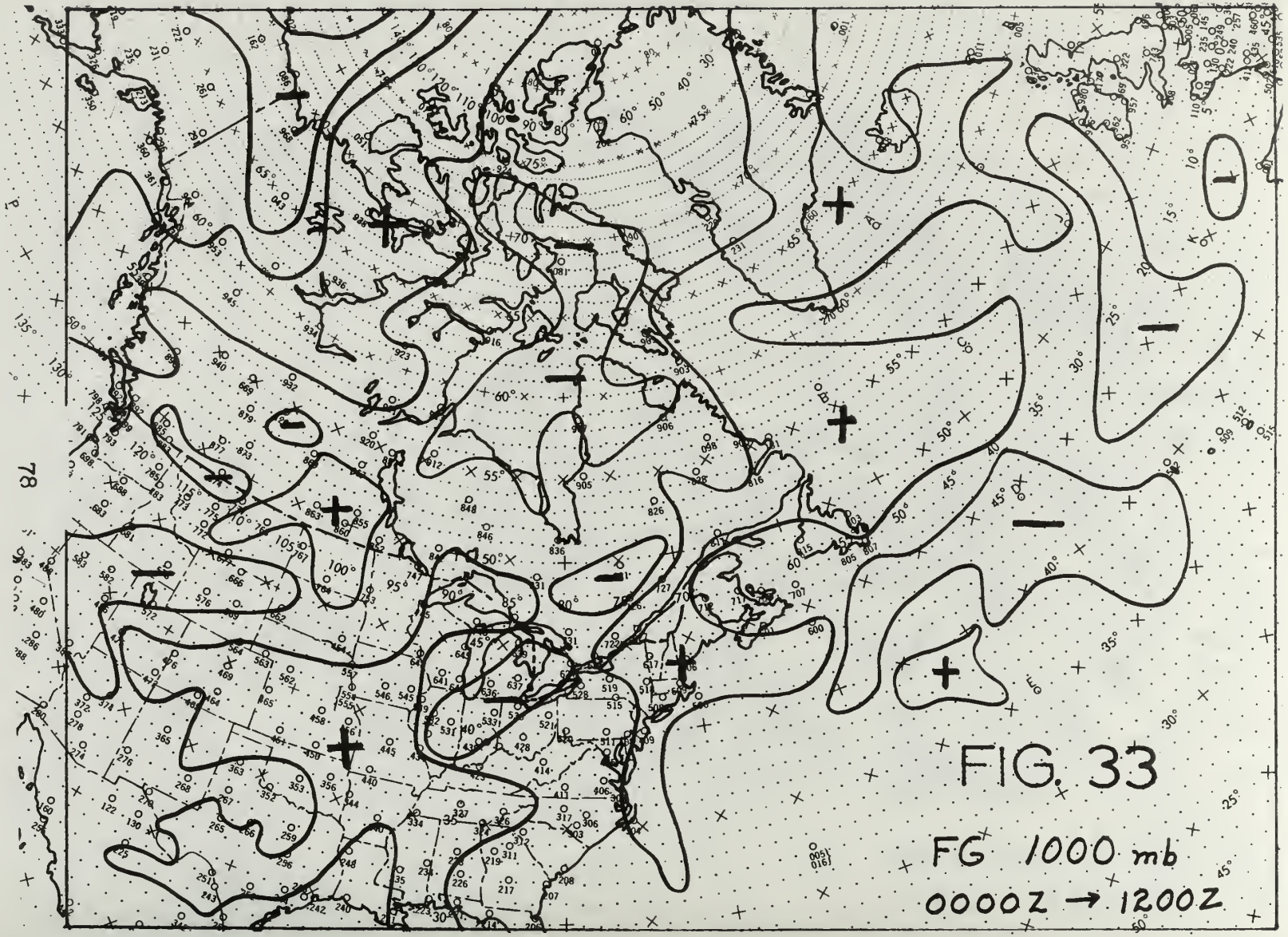
FIG. 33
FG 1000 mb
0000Z → 1200Z

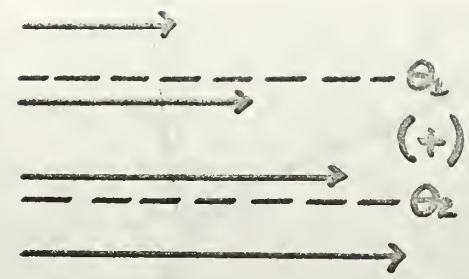

#1

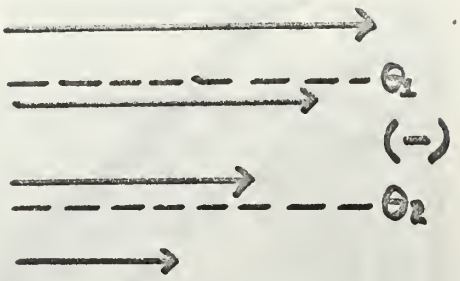

#2

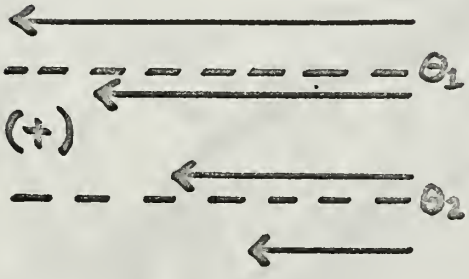

#3

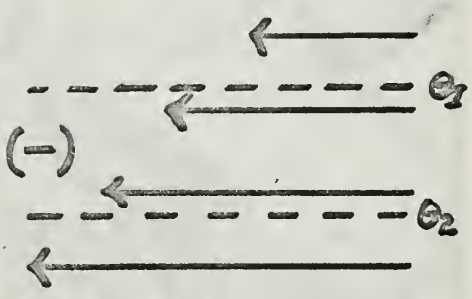

#4

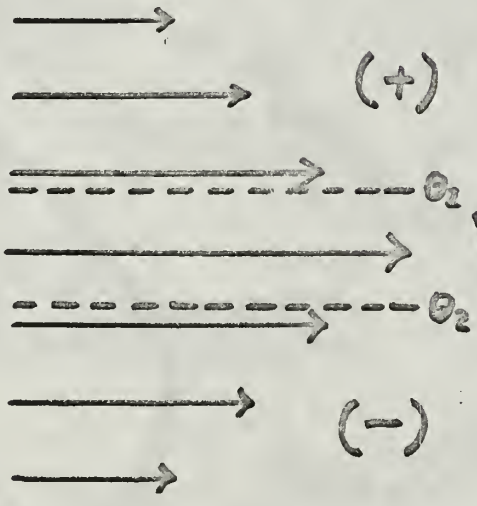

VFmax

#1 and #2

Fig 34

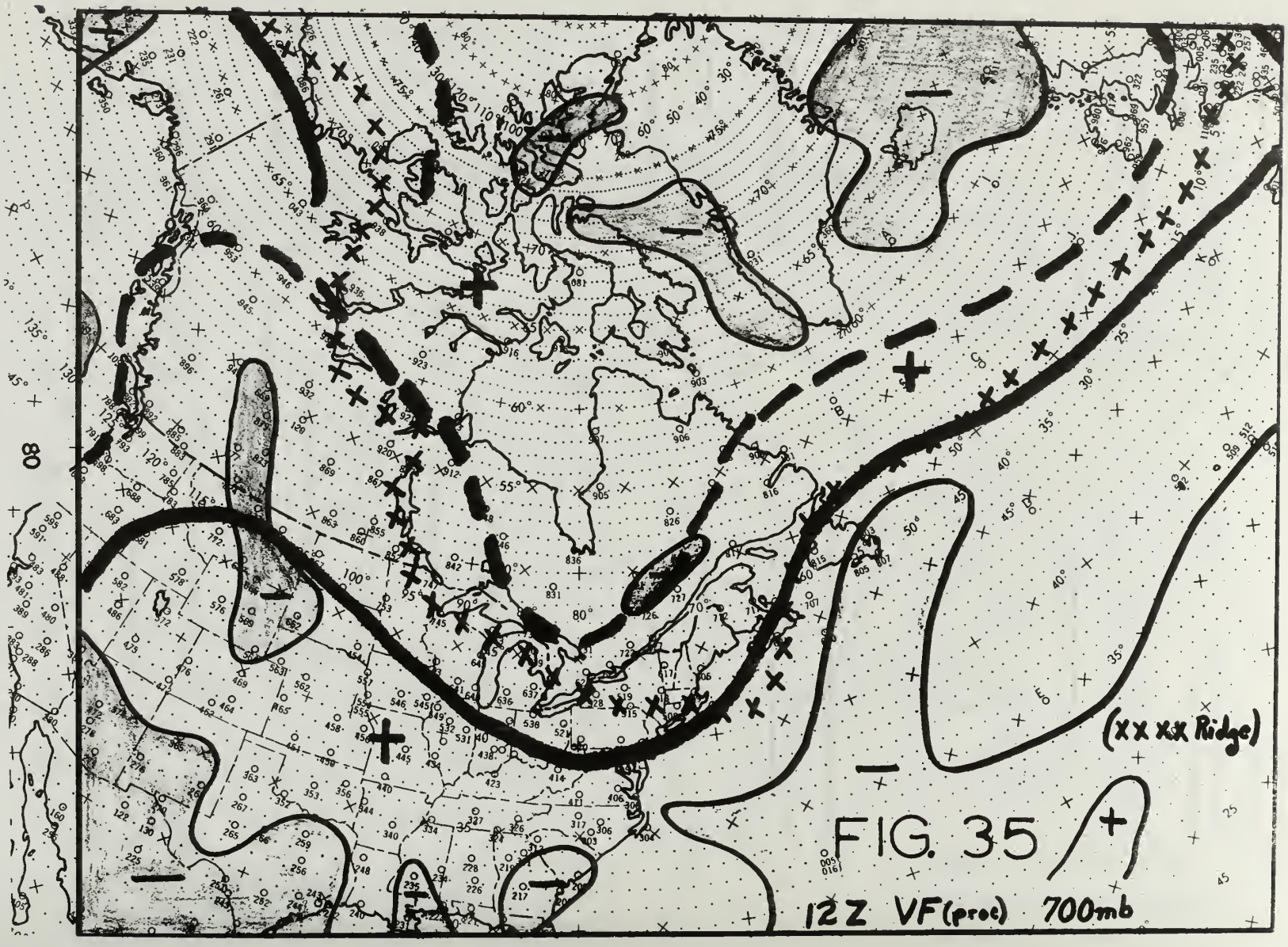
(XXXX Ridge)
FIG. 35
12Z VF(proc) 700mb

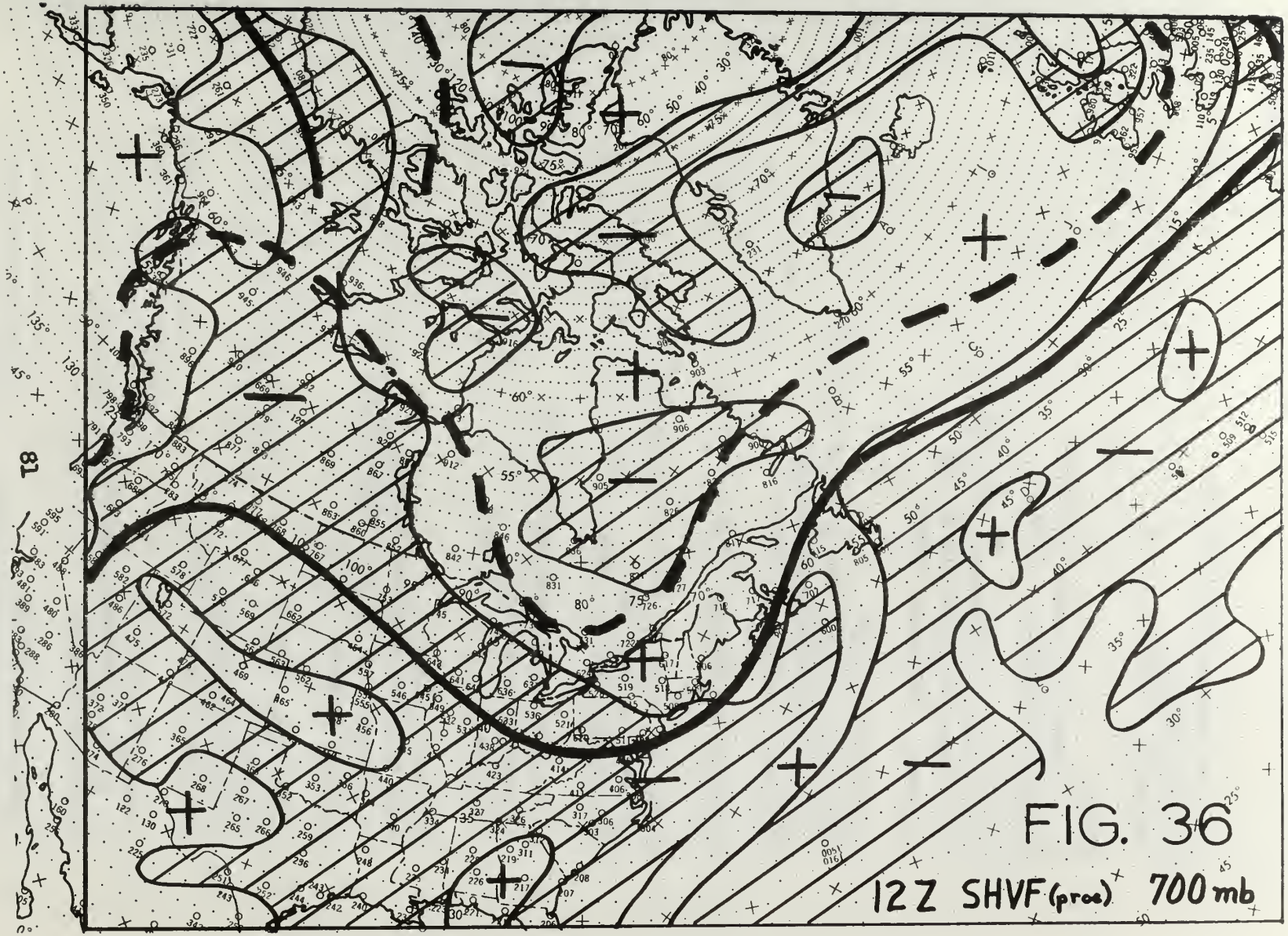

FIG. 36

12Z SHVF (proc) 700 mb

INITIAL DISTRIBUTION LIST

		No. Copies
1.	Defense Documentation Center Cameron Station Alexandria, Virginia 22314	20
2.	Library U. S. Naval Postgraduate School Monterey, California 93940	2
3.	Department of Meteorology & Oceanography U. S. Naval Postgraduate School Monterey, California 93940	1
4.	Professor R. Renard Department of Meteorology & Oceanography U. S. Naval Postgraduate School Monterey, California 93940	15
5.	LT Delvin L. Schardt, USN	2
6.	Office of the U. S. Naval Weather Service Washington Navy Yard Washington, D. C. 20390	1
7.	Chief of Naval Operations (Op-09B7) Department of the Navy Washington, D. C. 20350	1
8.	Officer in Charge Navy Weather Research Facility U. S. Naval Air Station, Bldg. R-48 Norfolk, Virginia 23511	1
9.	Commanding Officer FWC/JTWC COMNAVMARIANAS FPO San Francisco 96601	1
10.	Commanding Officer U. S. Fleet Weather Central FPO Seattle 98790	1
11.	Commanding Officer U. S. Fleet Weather Central FPO San Francisco 96610	1

12. Commanding Officer 1
U. S. Fleet Weather Central
FPO New York 09540

13. Commanding Officer 1
U. S. Fleet Weather Central
Navy Department
Washington, D. C. 20390

14. Commanding Officer 1
U. S. Fleet Weather Central
U. S. Naval Air Station
Alameda, California 94501

15. Commanding Officer and Director 1
Navy Electronics Laboratory
Attn: Code 2230
San Diego, California 92152

16. Officer in Charge 1
U. S. Fleet Weather Facility
FPO New York 09597

17. Officer in Charge 1
U. S. Fleet Weather Facility
FPO New York 09510

18. Officer in Charge 1
U. S. Fleet Weather Facility
FPO New York 09571

19. Officer in Charge 1
U. S. Fleet Weather Facility
FPO San Francisco 96662

20. Officer in Charge 1
U. S. Fleet Weather Facility
FPO San Francisco 96652

21. Officer in Charge 1
Fleet Weather Facility
U. S. Naval Air Station
San Diego, California 92135

22. Officer in Charge 1
Fleet Weather Facility
U. S. Naval Air Station
Quonset Point, Rhode Island 02819

REVISED DISTRIBUTION LIST

Main Library, USNPG Sch	~~8~~ 2
Author	3
Advisor	2
Dept of Met. and Oce., USNPG Sch	2
USN FNWF	2
Extra for future distribution (Dept. of Met. and Oce.)	~~18~~ 19

23. Officer in Charge — 1
Fleet Weather Facility
Box 85
U. S. Naval Air Station
Jacksonville, Florida 32212

24. Officer in Charge — 1
Fleet Numerical Weather Facility
U. S. Naval Postgraduate School
Monterey, California 93940

25. Director, Naval Research Laboratory — 1
Attn: Tech. Services Info. Officer
Washington, D. C. 20390

26. Office of Chief Signal Officer — 1
Research and Development Division
Department of the Army
Washington, D. C.

27. Commander — 1
Air Force Cambridge Research Center
(Attn: CROOTR)
Bedford, Massachusetts

28. Geophysics Research Directorate — 1
Air Force Cambridge Research Center
Cambridge, Massachusetts

29. Mr. Leo C. Clarke — 1
Fleet Numerical Weather Facility
U. S. Naval Postgraduate School
Monterey, California 93940

30. Program Director for Meteorology — 1
National Science Foundation
Washington, D. C.

31. Headquarters, 2nd Weather Wing (MAC) — 1
United States Air Force
APO #633
New York, New York

32. American Meteorological Society — 1
45 Beacon Street
Boston, Massachusetts

33. Commander, Air Weather Service — 2
Military Airlift Command
U. S. Air Force
Scott Air Force Base, Illinois 62226

34. U. S. Department of Commerce, ESSA — 2
Weather Bureau
Washington, D. C.

35. Office of Naval Research — 1
Department of the Navy
Washington, D. C. 20360

36. U. S. Naval Oceanographic Office — 1
Attn: Division of Oceanography
Washington, D. C. 20390

37. Chairman — 1
Department of Meteorology & Oceanography
New York University
University Heights, Bronx
New York, New York

38. Department of Meteorology — 1
University of California
Los Angeles, California

39. Department of the Geophysical Sciences — 1
University of Chicago
Chicago, Illinois

40. Department of Atmospheric Science — 1
Colorado State University
Fort Collins, Colorado

41. Department of Engineering Mechanics — 1
University of Michigan
Ann Arbor, Michigan

42. School of Physics — 1
University of Minnesota
Minneapolis, Minnesota

43. Department of Meteorology — 1
University of Utah
Salt Lake City, Utah

44. National Center for Atmospheric Research 1
Boulder, Colorado

45. Department of Meteorology and Climatology 1
University of Washington
Seattle, Washington 98105

46. Department of Meteorology 1
University of Wisconsin
Madison, Wisconsin

47. Department of Meteorology 1
Florida State University
Tallahassee, Florida

48. Department of Meteorology 1
Massachusetts Institute of Technology
Cambridge, Mass. 02139

49. Department of Meteorology 1
Pennsylvania State University
University Park, Pennsylvania

50. Department of Meteorology 1
San Jose State
San Jose, California

51. Hawaii Institute of Geophysics 1
University of Hawaii
Honolulu, Hawaii

52. University of Oklahoma 1
Research Institute
Norman, Oklahoma

53. Atmospheric Science Branch 1
Science Research Institute
Oregon State College
Corvallis, Oregon

54. The University of Texas 1
Electrical Engineering Research Laboratory
Engineering Science Bldg. 631A
University Station
Austin, Texas 78712

55. Department of Meteorology 1
Texas A&M University
College Station, Texas 77843

56. Weather Dynamics Group 1
Aerophysics Laboratory
Stanford Research Institute
Menlo Park, California

57. Meteorology International, Inc. 1
P. O. Box 1364
Monterey, California 93940

58. The Travelers Research Center, Inc.
650 Main Street
Hartford, Connecticut

59. United Air Lines 1
Director of Meteorology
P. O. Box 8800
Chicago, Illinois

60. Meteorology Section 1
Aracon Geophysics Co.
Virginia Road
Concord, Massachusetts 01742

61. Librarian 1
GCA Technology Division
GCA Corporation
Bedford, Massachusetts 01730

62. Department of Meteorology 1
University of Melbourne
Grattan Street
Parkville, Victoria
Australia

63. Bureau of Meteorology 1
Department of the Interior
Victoria and Drummond Streets
Carlton, Victoria
Australia

64. C. S. I. R. O. 1
Division of Meteorological Physics
Station Street
Aspendale, Victoria
Australia

65. Institut f. Meteor. u. Geophysik Universitat Innsbruck
Schopfstrassee 41, Innsbruck
Austria — 1

66. Department of Meteorology
McGill University
Montreal, Canada — 1

67. Central Analysis Office
Meteorological Branch
Regional Adm. Building
Inter. Airport
Dorval, Quebec, Canada — 1

68. Meteorological Office
315 Bloor Street West
Toronto 5, Ontario, Canada — 1

69. Department of Meteorology
University of Copenhagen
Copenhagen, Denmark — 1

70. Institute of Meteorology
University of Helsinki
Helsinki - Porthania, Finland — 1

71. Institut fur Theoretische Meteorologie
Freie Universitat Berlin
Berlin-Dahlem
Thiel-allee 49
Federal Republic of Germany — 1

72. Meteorological Institute
University of Thessaloniki
Thessaloniki, Greece — 1

73. Meteorological Service
44, Upper O'Connell Street
Dublin 1, Ireland — 1

74. Department of Meteorology
The Hebrew University
Jerusalem, Israel — 1

75. Geophysical Institute — 1
Tokyo University
Bunkyo-Ku
Tokyo, Japan

76. Meteorological Research Institute — 1
Kyoto University
Kyoto, Japan

77. Department of Astronomy and Meteorology — 1
College of Liberal Arts and Sciences
Seoul National University
Tong Soong Dong, Chong No Ku
Seoul, Korea

78. Central Meteorological Office — 1
I Song Wul Dong, Sudaemon Ku
Seoul, Korea

79. Department of Meteorology — 1
Instituto de Geofisica
Universidad Nacional de Mexico
Mexico 20, D. F., Mexico

80. New Zealand Meterological Service — 1
P. O. Box 722
Wellington, G. E. New Zealand

81. Institutt for Teoretisk Meteorologi — 1
University of Oslo
Blindern, Oslo, Norway

82. Institute of Geophysics — 1
University of Bergen
Bergen, Norway

83. Pakistan Meteorological Department — 1
Institute of Meteorology and Geophysics
Karachi, Pakistan

84. Royal Swedish Air Force — 1
M. V. C.
Stockholm 80, Sweden

85. Department of Meteorology — 1
Imperial College of Science
South Kensington
London S.W. 7, United Kingdom

86. Meteorological Office 1
London Rd.
Bracknell
Berkshire, United Kingdom

87. National Research Institute for 1
Mathematical Sciences
C. S. I. R.
P. O. Box 395
Pretoria, Union of South Africa

DOCUMENT CONTROL DATA - R&D

(Security classification of title, body of abstract and indexing annotation must be entered when the overall report is classified)

1. ORIGINATING ACTIVITY *(Corporate author)*

U. S. Naval Postgraduate School
Monterey, California 93940

2a. REPORT SECURITY CLASSIFICATION
UNCLASSIFIED

2b. GROUP

3. REPORT TITLE

A CASE STUDY OF DATA PROCESSING AND WIND PARAMETERS IN RELATION TO THE U. S. NAVY'S NUMERICAL FRONTAL ANALYSIS SCHEME

4. DESCRIPTIVE NOTES *(Type of report and inclusive dates)*
Thesis

5. AUTHOR(S) *(Last name, first name, initial)*
Schardt, Delvin L., Lieutenant, U. S. Navy

6. REPORT DATE	7a. TOTAL NO. OF PAGES	7b. NO. OF REFS
May 1966	90	9

8a. CONTRACT OR GRANT NO.	9a. ORIGINATOR'S REPORT NUMBER(S)
NA	NA
b. PROJECT NO.	
c.	9b. OTHER REPORT NO(S) *(Any other numbers that may be assigned this report)*
d.	NA

10. AVAILABILITY/LIMITATION NOTICES

Qualified requesters may obtain copies of this report from DDC.

11. SUPPLEMENTARY NOTES	12. SPONSORING MILITARY ACTIVITY
NA	Chief of Naval Operations (Op-09B7) Department of the Navy Washington, D. C. 20350

13. ABSTRACT

The United States Navy's (USN) numerical front-location parameter, as developed by Renard and Clarke, is investigated in its relation to the data-processing system used at the USN Fleet Numerical Weather Facility (FNWF) Monterey, California, and to three front-associated wind parameters: a) geostrophic wind normal to isentropes, b) shear of geostrophic wind tangent to isentropes, and c) a frontogenetical parameter. The study is carried out for the Northern Hemisphere at 1000, 850, 700, 500, and 300 mb for 00Z and 12Z, 20 August 1965, in the framework of FNWF's numerical analysis system.

Results indicate some major differences between the synoptic-scale baroclinic zones analyzed from radiosonde-observed temperatures, and FNWF's numerically processed mandatory-level virtual temperature data, at 1000 mb, over ocean areas, and at latitudes north of 55 degrees latitude. The normal geostrophic wind component was found to be useful in designating the type of front; (cold, warm, stationary). Frontal shear proved to be mostly cyclonic at low levels (1000, 850 mb) becoming increasingly anticyclonic at higher levels (700, 500, 300 mb). The advective frontogenesis parameter appeared to be of limited value.

14. KEY WORDS	LINK A		LINK B		LINK C	
	ROLE	WT	ROLE	WT	ROLE	WT
NUMERICAL FRONT-LOCATION PARAMETER GEOSTROPHIC WIND NORMAL TO ISENTROPES GEOSTROPHIC WIND TANGENT TO ISENTROPES FRONTOGENETICAL PARAMETER						

INSTRUCTIONS

1. ORIGINATING ACTIVITY: Enter the name and address of the contractor, subcontractor, grantee, Department of Defense activity or other organization *(corporate author)* issuing the report.

2a. REPORT SECURITY CLASSIFICATION: Enter the overall security classification of the report. Indicate whether "Restricted Data" is included. Marking is to be in accordance with appropriate security regulations.

2b. GROUP: Automatic downgrading is specified in DoD Directive 5200.10 and Armed Forces Industrial Manual. Enter the group number. Also, when applicable, show that optional markings have been used for Group 3 and Group 4 as authorized.

3. REPORT TITLE: Enter the complete report title in all capital letters. Titles in all cases should be unclassified. If a meaningful title cannot be selected without classification, show title classification in all capitals in parenthesis immediately following the title.

4. DESCRIPTIVE NOTES: If appropriate, enter the type of report, e.g., interim, progress, summary, annual, or final. Give the inclusive dates when a specific reporting period is covered.

5. AUTHOR(S): Enter the name(s) of author(s) as shown on or in the report. Enter last name, first name, middle initial. If military, show rank and branch of service. The name of the principal author is an absolute minimum requirement.

6. REPORT DATE: Enter the date of the report as day, month, year; or month, year. If more than one date appears on the report, use date of publication.

7a. TOTAL NUMBER OF PAGES: The total page count should follow normal pagination procedures, i.e., enter the number of pages containing information.

7b. NUMBER OF REFERENCES: Enter the total number of references cited in the report.

8a. CONTRACT OR GRANT NUMBER: If appropriate, enter the applicable number of the contract or grant under which the report was written.

8b, 8c, & 8d. PROJECT NUMBER: Enter the appropriate military department identification, such as project number, subproject number, system numbers, task number, etc.

9a. ORIGINATOR'S REPORT NUMBER(S): Enter the official report number by which the document will be identified and controlled by the originating activity. This number must be unique to this report.

9b. OTHER REPORT NUMBER(S): If the report has been assigned any other report numbers *(either by the originator or by the sponsor)*, also enter this number(s).

10. AVAILABILITY/LIMITATION NOTICES: Enter any limitations on further dissemination of the report, other than those imposed by security classification, using standard statements such as:

(1) "Qualified requesters may obtain copies of this report from DDC."

(2) "Foreign announcement and dissemination of this report by DDC is not authorized."

(3) "U. S. Government agencies may obtain copies of this report directly from DDC. Other qualified DDC users shall request through

_____."

(4) "U. S. military agencies may obtain copies of this report directly from DDC. Other qualified users shall request through

_____."

(5) "All distribution of this report is controlled. Qualified DDC users shall request through

_____."

If the report has been furnished to the Office of Technical Services, Department of Commerce, for sale to the public, indicate this fact and enter the price, if known.

11. SUPPLEMENTARY NOTES: Use for additional explanatory notes.

12. SPONSORING MILITARY ACTIVITY: Enter the name of the departmental project office or laboratory sponsoring *(paying for)* the research and development. Include address.

13. ABSTRACT: Enter an abstract giving a brief and factual summary of the document indicative of the report, even though it may also appear elsewhere in the body of the technical report. If additional space is required, a continuation sheet shall be attached.

It is highly desirable that the abstract of classified reports be unclassified. Each paragraph of the abstract shall end with an indication of the military security classification of the information in the paragraph, represented as *(TS)*, *(S)*, *(C)*, or *(U)*.

There is no limitation on the length of the abstract. However, the suggested length is from 150 to 225 words.

14. KEY WORDS: Key words are technically meaningful terms or short phrases that characterize a report and may be used as index entries for cataloging the report. Key words must be selected so that no security classification is required. Identifiers, such as equipment model designation, trade name, military project code name, geographic location, may be used as key words but will be followed by an indication of technical context. The assignment of links, roles, and weights is optional.